UNCLASSIFIED

AD 106290

Armed Services Technical Information Agency

Reproduced by

DOCUMENT SERVICE CENTER

KNOTT BUILDING, DAYTON, 2, OHIO

UNCLASSIFIED

FC

Design Considerations

For Pencil Type Air Blast Gages

Prepared for

BALLISTIC RESEARCH LABORATORIES

Aberdeen Proving Ground, Maryland

Under

Contract No. DA-36-034-ORD-1860

November 1, 1955

Prepared by

ATLANTIC RESEARCH CORPORATION

Alexandria, Virginia

DESIGN CONSIDERATIONS FOR

PENCIL TYPE AIR BLAST GAGES

James W. Fitzgerald

Prepared For

Ballistic Research Laboratories
Aberdeen Proving Ground, Maryland

Contract No. DA-36-034-ORD-1860
Atlantic Research Corporation Purchase Order No. 20172

Department of the Army Project No. 5B0306011
Ordnance Corps Project No. TB3-0538

November 1, 1955

ATLANTIC RESEARCH CORPORATION

PREFACE

Much of the work reported herein was done by the author while Director
of the Electromechanical Division of the Atlantic Research Corporation in
Alexandria, Virginia. The development effort there was sponsored by the
Ballistic Research Laboratories of the Aberdeen Proving Ground in a series
of contracts (1, 2, 3)[*] extending from January 1952, through February 1955.
A general summary (4) of all of the air blast gage development done during
that period has been compiled from progress reports issued under the contracts
and reference is made to that Technical Review Report for details of some of the
other work.

The present report is concerned for the main part with a detailed
description of the characteristics of one of the gage types developed during
this period. Its design is based on a streamlined, pencil-shaped, housing
and on the use of a barium titanate cylinder as the sensitive element. The
basic electroacoustic system had been previously developed by the author in
connection with a sonar transducer application (5) and was adapted to the air
blast problem.

It was felt necessary to set the scene, so to speak, for some of the
design considerations that have led to the general features of the Pencil
Gage by digressing into the separate fields of Aerodynamics and Electroacoustics.
It is hoped that those versed in these fields will be indulgent with a somewhat
limited presentation. Some of the more mature reflections on the problem of
air blast pressure measurement have resulted from a continuing interest in the
field since leaving Atlantic Research Corporation. This interest has had the
advantage of being unhampered from specific assignment but in turn has suffered
from the press of other work. In retrospect and review, the author holds the
view that much of the work, past and present, in the domain of air blast
measurement and gage design is prejudiced by misinformation resulting from
a naive and superficial approach to the problem. Perhaps in some small
measure the material presented herein will contribute a step toward putting
air blast transient pressure measurement on a firmer foundation.

---

[*] Numbers in parentheses refer to the references at the end of the report.

It is with considerable pleasure that I acknowledge the many contributions to these studies by my able colleagues of that period, F. P. Clay, Jr., H. Marron, C. W. Ward, and G. C. Pierce. S. T. Marks, as Technical Supervisor from the Ballistic Research Laboratories, has given unflagging encouragement to the work. Personnel of the Ballistic Research Laboratories have also made important contributions, including some of the data and photographs contained herein.

J. W. Fitzgerald
Chesapeake Instrument Corporation
Shadyside, Maryland
November 1, 1955

4

TABLE OF CONTENTS

LIST OF FIGURES

LIST OF FIGURES

I. INTRODUCTION

Measurements of transient pressures associated with blast or shock waves pro-
pagated in gaseous media impose stringent requirements on transducer designs that
are not usually encountered in most electroacoustic devices. Reasonably accurate
reproduction of shock pressure transients requires a flat frequency response from
a fraction of a cycle per second to one hundred kilocycles per second, or higher.
Pressure peaks encountered may be several hundreds of pounds per square inch.
Field testing conditions are rugged, and pyroelectric effects due to compressive
heating of the shock front must be avoided. Super-imposed on these difficulties
are aerodynamic effects of the interaction of the gage and its housing with the
oncoming shock wave which can greatly perturb the local pressure field.

Most of these difficulties can be overcome through proper application of
aerodynamic considerations to the transducer design problem. This report briefly
summarizes the conditions existing in the blast field as they apply to the
measurement problem; reviews their effects on earlier gage designs; demonstrates
how the use of streamlined gage housings can minimize perturbations of the local
pressure field; and shows how properly designed electroacoustic elements can yield
accurate reproductions of shock wave pressures.

The so-called pencil gage described in this report is based on the use of a
piezoelectric barium titanate cylindrical shell mounted in, but electrically and
mechanically isolated from, a pencil-shaped streamlined housing. A neoprene cover
bonded both to the active face of the titanate and to the housing protects the
cylinder from its environment and minimizes pyroelectric effects of the blast
wave. The nose of the gage, in use, is pointed toward the blast. The shock wave
propagates normally over the streamlined housing without appreciable disturbance,
and the sensitive element measures the transverse pressure of the shock wave.
The measured pressure corresponds very nearly to the free-field pressure of the
wave.

II. AERODYNAMIC FACTORS IN GAGE DESIGN

There are a number of aerodynamic considerations that enter into the design
of an air blast gage. The basic problem is one of designing a housing for the
sensitive element that does not unduly disturb the shock wave and presents to
the active surface of the sensitive element a pressure-time relation that is
substantially indentical with that of the free-field or undisturbed shock. The
problem becomes increasingly acute at the higher peak pressures.

9

A. Description of the Blast Field

The first disturbance in the air surrounding an exploding spherical charge is due to the arrival of the detonation wave at the surface of the reacting explosive. The pressure, which is of the order of two million pounds per square inch (6) for TNT, begins to be relieved by an intense compression wave propagating outward and by an outward flow of air. The dense mass of gaseous combustion products left upon completion of the detonation continues to expand outward and the pressure falls off rapidly. For all practical purposes the pressure rise is discontinuous and is followed by a roughly exponential decay with a duration from a few milliseconds to several seconds, depending on the size of the charge.

Disturbances of this kind differ greatly from the essentially linear phenomena of ordinary sound waves and are governed by nonlinear differential equations (7, 8). As a consequence, the usual laws of superposition, reflection and refraction are no longer applicable. As it propagates outward, the initial discontinuity (called a "shock front") resulting from the blast causes sudden and violent changes in particle velocity, pressure, and temperature in the medium. A number of qualitative differences between shock waves and acoustic waves (i.e., waves of infinitesimal amplitude) are a consequence of the non-linear characteristics of the former. In linear wave motion, initial discontinuities are preserved and propagated with a definite "sonic" velocity which is a local property of the medium. In nonlinear wave motion, however, discontinuities may either be resolved or built up to one or more shock fronts and are propagated at "supersonic" velocities relative to the medium ahead. The pressure level in spherical shock waves falls off more rapidly than the inverse first power law predicted for small amplitudes but eventually approaches this as the amplitude becomes small (See Figure 1). Excess pressures of interfering sound waves are simply additive, but the interaction and reflection of shock waves can lead to large increases in pressures. This last phenomenon is of considerable consequence in the problem of shock wave measurement.

The important Rankine-Hugoniot equation (9) relates the peak pressure of a shock front and its velocity of propagation as follows:

$$P_s = P_o(\frac{2\gamma}{\gamma+1}) \cdot (\frac{V^2}{c_o^2} - 1) , \tag{1}*$$

where P_s is the peak pressure above atmospheric pressure,

P_o is the atmospheric pressure ahead of the shock,

---

*Eq. (1) is valid for peak pressures below 300 psi where air behaves like a perfect gas.
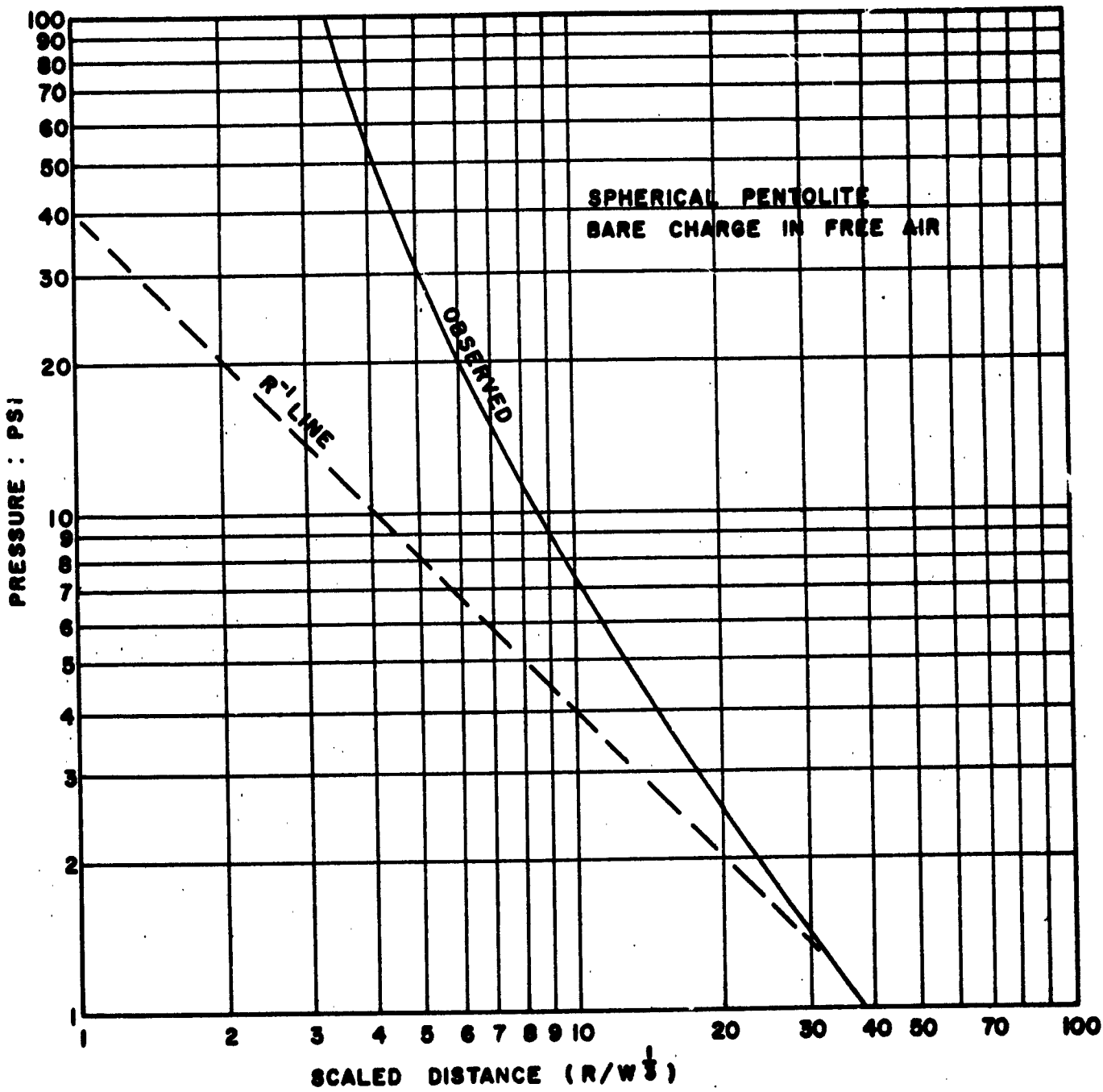
FIGURE 1: PEAK PRESSURE AS A FUNCTION OF SCALED
DISTANCE. (BRL DATA)

R = DISTANCE FROM CHARGE (FT)
W = WEIGHT OF CHARGE (LBS)

V is the velocity of shock-front propagation,

C_o is the velocity of sound in air ahead of the shock, and

γ is 1.40 (ratio of specific heats for air).

This equation is the basis for the calibration of air blast gages, since an independent measurement of the velocity of the shock front yields a value for the peak pressure.

B. Interaction of the Shock Wave and Plane Rigid Surfaces

The measurement of the excess pressure of a shock wave entails fundamentally two different phases. The first of these is the aerodynamic problem of devising a means of applying a pressure-time function identical with the free-field values to the active surface of the gage sensing element. The second phase is a matter of electroacoustical transducer design to achieve an electrical output that is a faithful replica of the applied pressure transient. We have a three-dimensional field problem in nonlinear gas dynamics and a one-dimensional linear problem in electroacoustic transduction. Any disregard of the separate requirements of the two scientific disciplines is certain to cause trouble.

The simple method of disposing the active surface of a plane circular transducer, to face an oncoming shock wave, is not a fruitful approach to the measurement of the free-field pressure. If we consider the geometry of Figure 2-a, assuming for simplicity that the gage is mounted in an infinite, rigid baffle, the determination of the pressure across the face of the gage becomes a matter of considering the reflection of a shock at a rigid wall at normal incidence. The sequence is clarified by diagramming events in the (x, t) plane as shown in Figure 2-b. Under the impact of the incident shock the undisturbed zone between the gage surface and the oncoming shock shrinks to zero at time $t = 0$, the moment of impact. Thereafter a reflected shock starts in the opposite direction, leaving behind a growing zone of quiet. It can be shown (10) that the ratio of excess pressure of the reflected to the incident shock is given by

$$\frac{P_r}{P_1} = 1 + \frac{1 + (\frac{\gamma-1}{\gamma+1})}{\frac{P_o}{P_1+P_o} + (\frac{\gamma-1}{\gamma+1})} \tag{2}$$

where γ is the ratio of specific heats of the medium,

P_o is the pressure in the medium before the incident shock,

P_1 is the peak excess pressure of the incident shock, and

P_r is the peak excess pressure of the reflected shock.

Figure 3 is a plot of Equation (2) for air ($\gamma = 1.4$). Clearly, the reflection of a shock at normal incidence on the gage surface results in considerable increase of pressure over that of the free-field shock pressure. The maximum
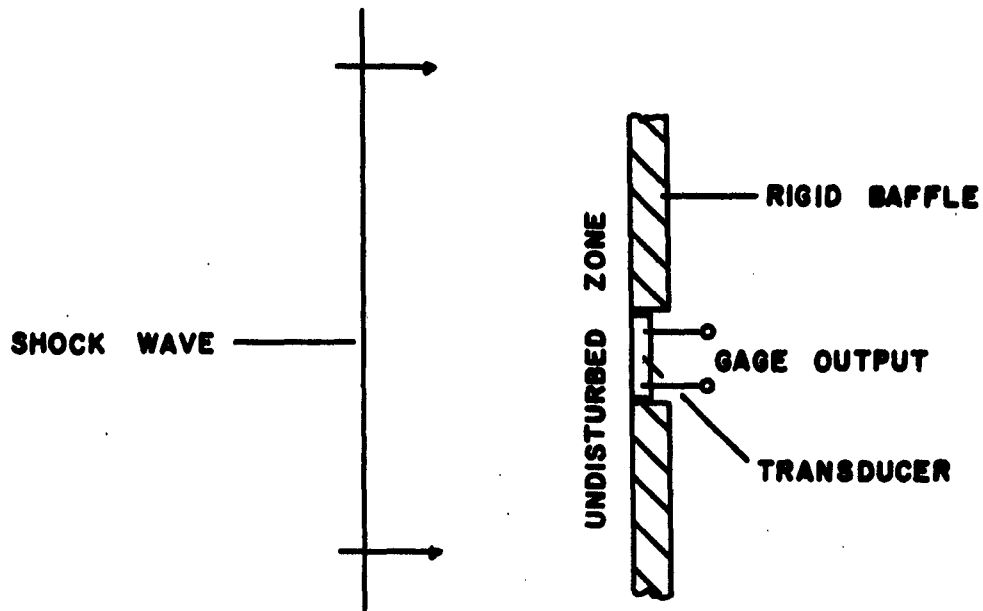
a. SHOCK WAVE APPROACHING
   HEAD-ON TO GAGE.
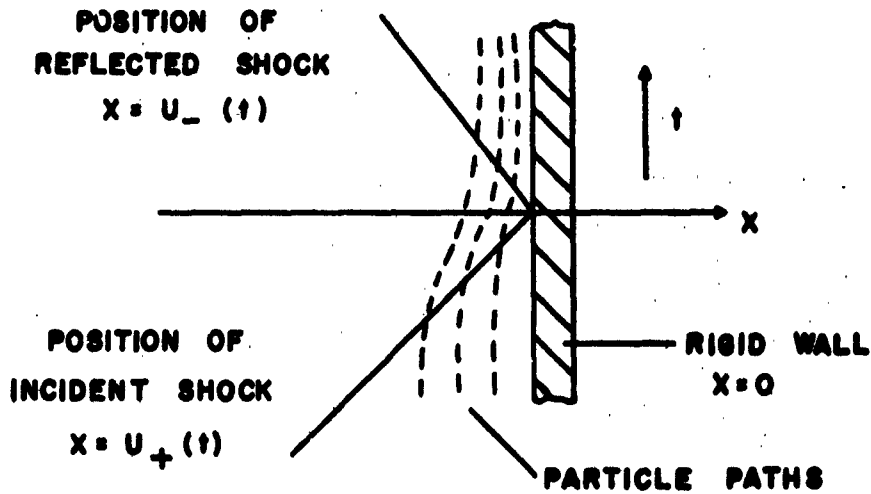
b. NORMAL REFLECTION OF A
   SHOCK AT A RIGID WALL.
   (AFTER COURANT)

FIGURE 2 : NORMAL REFLECTION OF A SHOCK AT
           A GAGE FACE.
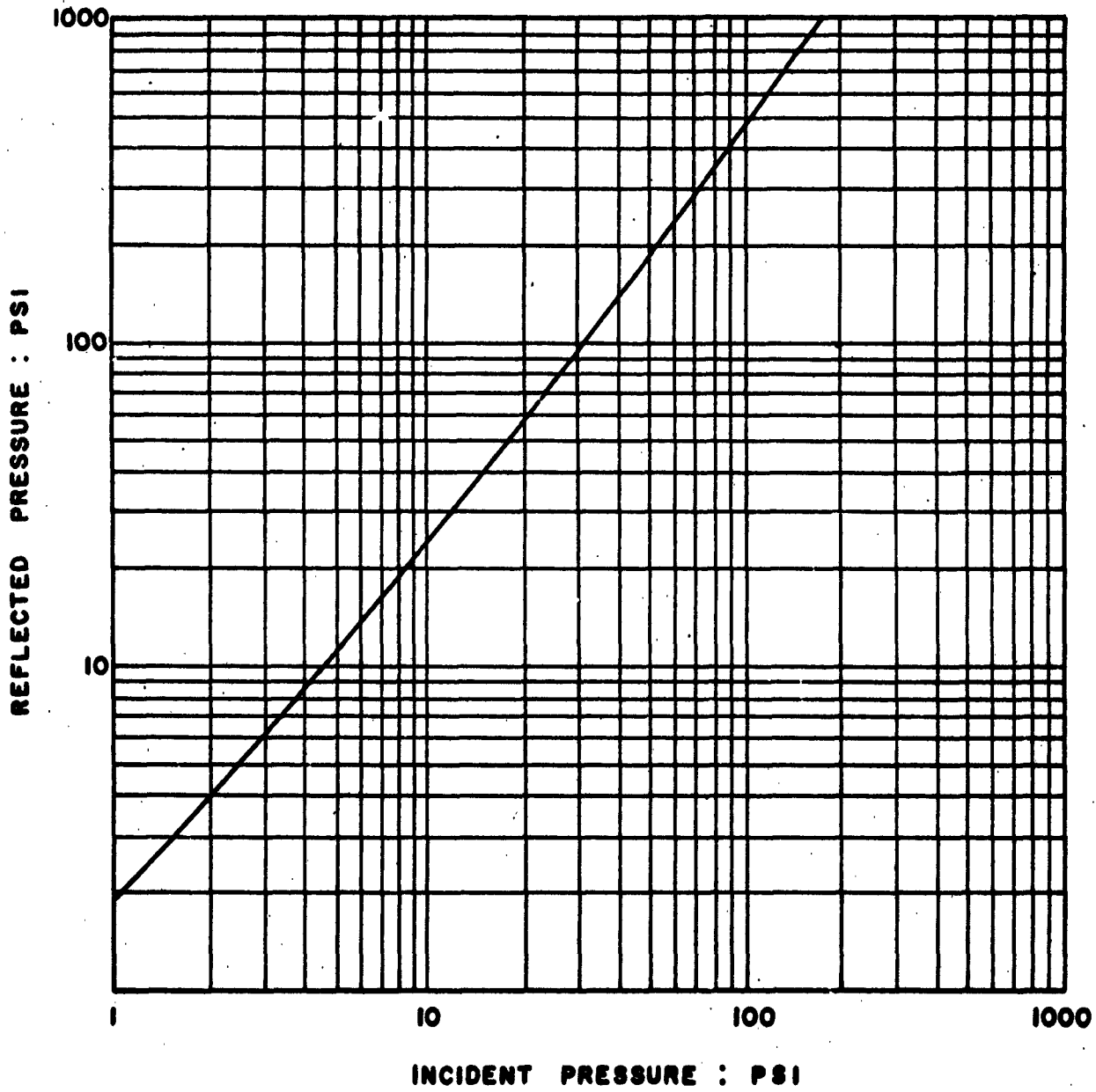
FIGURE 3: REFLECTED VS. INCIDENT PRESSURE
FOR A NORMAL SHOCK. (AFTER LAMPSON)

increase for strong shocks, when air behaves like a perfect gas, is approximately eight times the free-field value. For weak shocks, the value approaches the sonic reflection ratio of two. Nor is the situation improved for oblique incidence. In this case the reflected shock strength depends in a complex way on the angle of incidence and the strength of the incident shock (11). As the angle of incident shock (11). As the angle of incidence increases, the reflected pressure first decreases and then increases again, attaining the head-on value for an angle of about 39° in air. Beyond this angle the pressure ratio, in cases of weak or moderate shocks, rises above the head-on value. For strong shocks, on the other hand, oblique reflection never results in pressures as high as those for normal incidence.

From the standpoint of shock pressure measurements this is a rather discouraging picture. Fortunately, for the limiting angle of incidence of 90°, with the shock front traveling along the gage surface as shown in Figure 4-a, the pressure on the surface is essentially equal to the free-field pressure for all shock intensities.[*] As a consequence, it is seen that any pressure gage intended for free-field shock wave measurements must be designed to measure the transverse pressure of the shock.

There is still another propagative phenomenon that effects a modification of the pressure-time input to the gage. This is a consequence of the finite size of the sensitive element and results in an averaging effect, as can be seen from Figure 4-b. The effect is somewhat analogous to the diffraction problem in steady-state sinusoidal fields. Arons and Cole (12) have made a simple analysis for the response of a circular gage to a saw-tooth transient pressure wave. They assume a linear function as a sufficient approximation to the initial decay of a shock wave. For an incident wave of the form

$$P(x,t) = \begin{cases} 0, & \text{when } t < \dfrac{x}{c} \\ P_0 \left[1 - \dfrac{1}{\theta} \left(t - \dfrac{x}{c}\right)\right] & \text{when } t > \dfrac{x}{c} \end{cases} \qquad (3)$$

they obtain for the relative response of the gage:

---

[*] Boundary layer effects probably cause some pressure variation in the immediate neighborhood of the gage surface. This is negligible in most instances.

SHOCK WAVE

DISTURBED ZONE | UNDISTURBED ZONE

TRANSDUCER — RIGID WALL
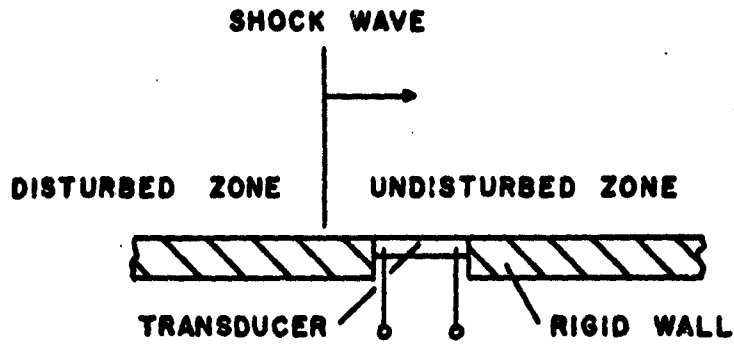
a. SHOCK TRAVELING ACROSS GAGE
   AT 90° INCIDENCE.

t_1 t_1 t_2 t_3

p | x

DISTURBED ZONE   UNDISTURBED ZONE

TRANSDUCER — RIGID WALL
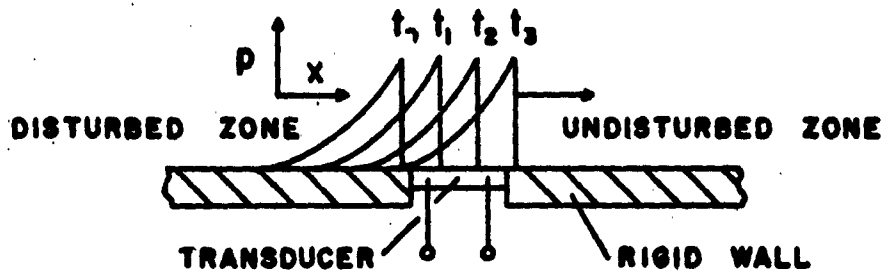
b. EXPONENTIAL PRESSURE PULSE
   TRAVELING ACROSS GAGE SURFACE.

p | x

DISTURBED ZONE   UNDISTURBED ZONE

RIGID WALL
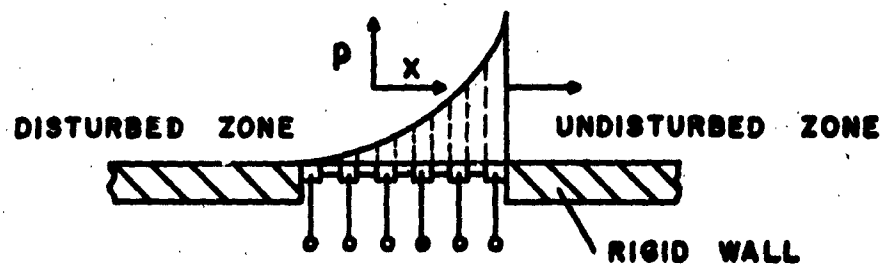
c. SEGMENTED TRANSDUCER FOR STUDYING
   TRANSIT TIME PHENOMENA.

FIGURE 4 : SHOCK TRAVERSING GAGE
             AT 90° INCIDENCE.

$$S(t) = \begin{cases} 0, & \text{for } t < -\dfrac{a}{c} \\[2mm] \dfrac{\phi}{\pi} - \dfrac{\sin\phi \cos\phi}{\pi} - \dfrac{a}{c\theta}\left(\dfrac{\sin\phi}{\pi} - \dfrac{\phi\cos\phi}{\pi} - \dfrac{\sin^3\phi}{3\pi}\right) & \\[2mm] 1 - \dfrac{t}{\theta} & \text{for } -\dfrac{a}{c} < t < \dfrac{a}{c} \\[2mm] & \text{for } t > \dfrac{a}{c} \end{cases} \quad (4)$$

In Equations (3) and (4) the symbols have the following definitions:

$P(x,t)$ is the instantaneous pressure, a function of distance x and time t;

P_o is the initial pressure;

θ is the decay constant;

c is the propagation velocity of the wave

$S(t)$ is the relative response of the gage, a function of time t;

a is the radius of the gage; and

ϕ is $\cos^{-1}(-\dfrac{ct}{a})$

Equation (4), giving the response of a gage to a saw-tooth pressure pulse, is plotted in Figure 5 as a function of $\dfrac{t}{\theta}$ for various values of the ratio $\dfrac{a}{c\theta}$. It is evident that the averaging effect of transit time can introduce an appreciable error.

Further insight into the problem could probably be obtained through experimental shock-tube studies with use of a segmented transducer as shown in Figure 4-c. Relative errors obtained by successively connecting additional segments in parallel would be useful data. The recorded gage outputs could be correlated with simultaneous photographs of the shock propagating across the gage surface. Frequency limitations in the transducer or associated electronic circuitry can introduce a similar rounding-off of the peak pressure; so, in studies of this type, care should be taken to design a system of high enough frequency response that the observed error can definitely be ascribed to transit time.

C. Gage Housing Designs

Although subject to some variation, there are three basic types of housing shapes that have been used for air blast gage designs with a view toward measuring the side-on pressure. Figure 6 is a photograph of the three types and Figure 7 is a sketch giving a cross-sectional view of each type. The first of these has a pillbox shaped housing and uses a tourmaline disc imbedded in an
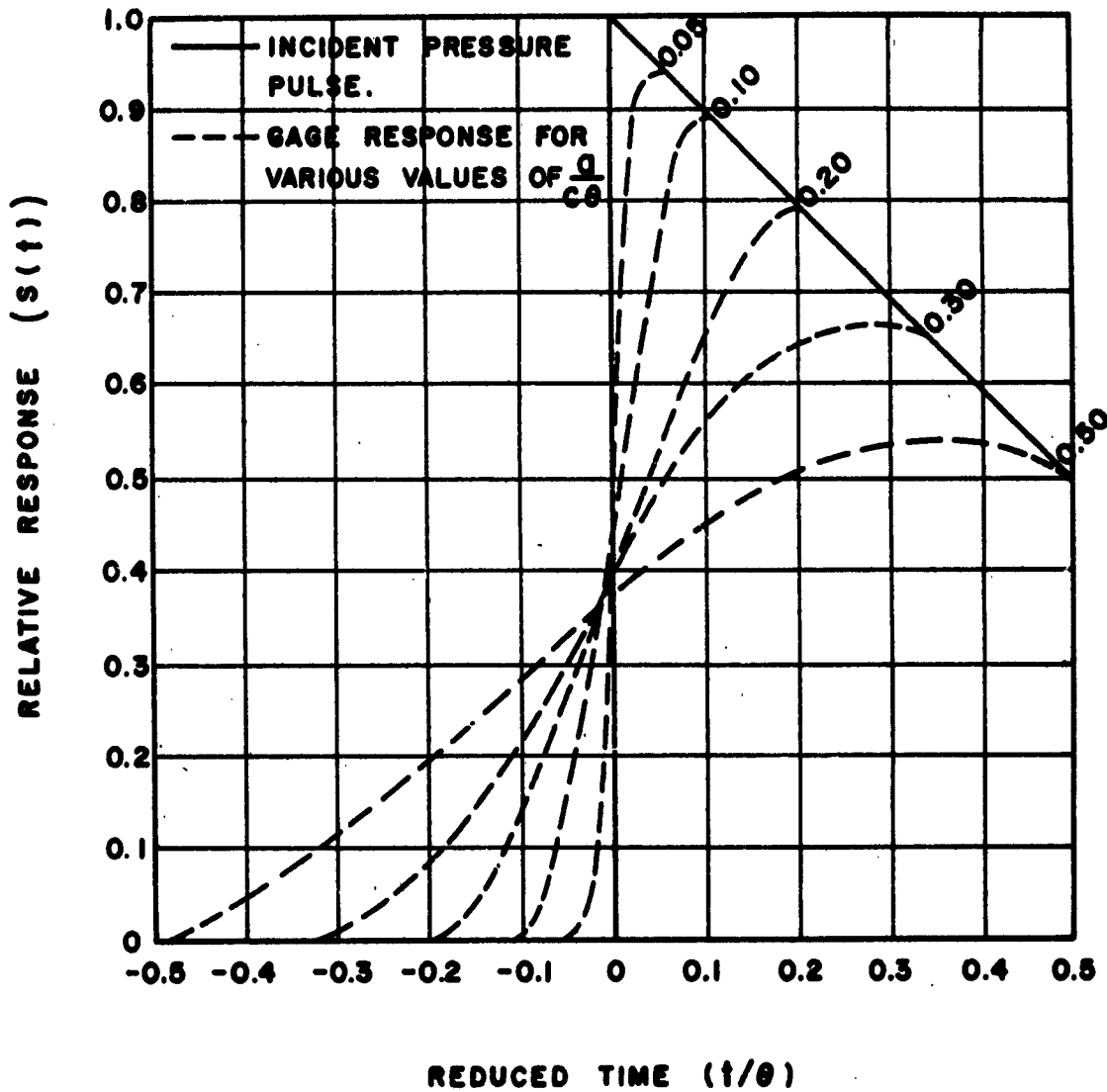
FIGURE 5: TRANSIT TIME ERROR FOR A
SAWTOOTH TRANSIENT. (AFTER COLE)

18
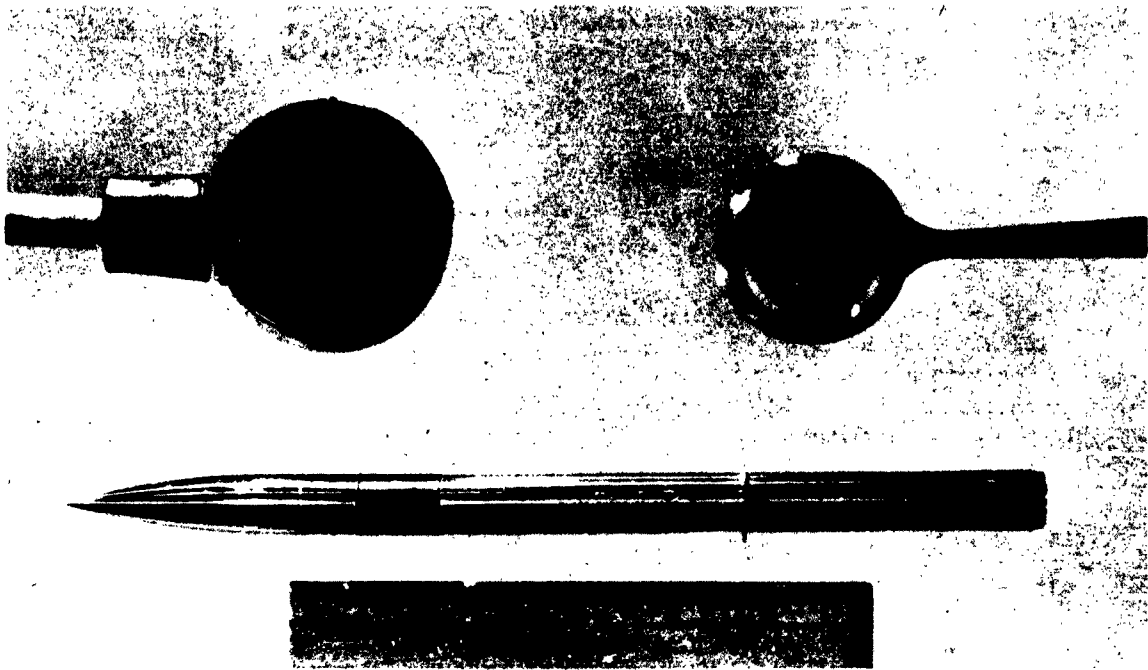
PILLBOX PANCAKE PENCIL
UPPER LEFT UPPER RIGHT LOWER CENTER

FIGURE 6: BASIC AIR BLAST GAGE DESIGNS.
(BRL PHOTOGRAPH)
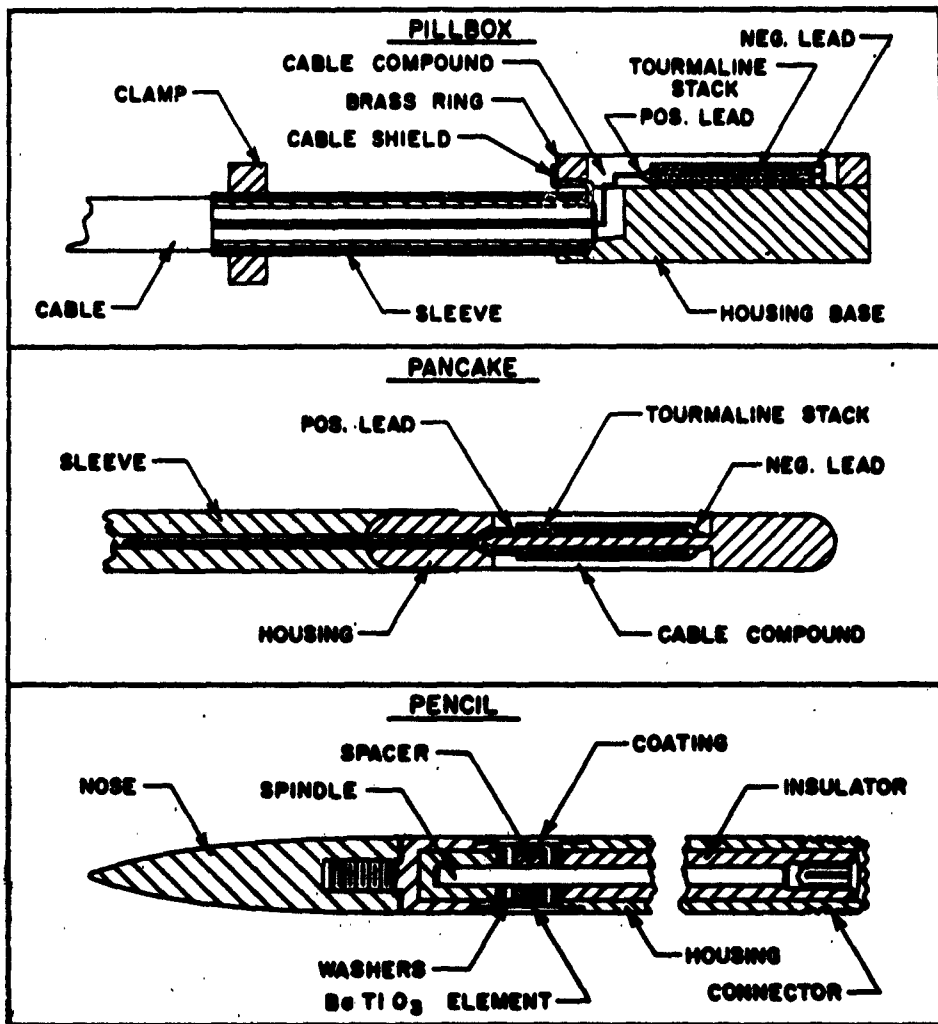
FIGURE 7: CROSS-SECTION VIEW OF BASIC AIR
BLAST GAGE DESIGNS. (BRL SKETCH)

asphaltic compound. Units of this type were developed at the Ballistic Research Laboratories during the latter part of World War II (13) and most of the blast measurements made during, and immediately following, that period used gages of this type. With the realization that a more streamlined housing would give better results (14, 15), gages of the "pancake" type were developed. Both tourmaline and barium titanate sensitive elements have been used in housings of this type. Finally, the so-called pencil gage was evolved (16) giving a highly streamlined housing usable up to high peak pressures.

D. Shock Tube Studies of Gage Shapes

Some preliminary studies of the flow around gage housings have been made in the 4-inch shock tube at the Ballistic Research Laboratories. Perturbations in the flow pattern that develop around a pillbox type housing are demonstrated by the series of shadowgraphs shown in Figure 8. The photographs represent four separate runs at peak pressures of about 12.5 psi. Double exposures of approximately 25 microseconds separation were taken at successively later times in order to observe the shock at several positions along the gage. In the first photograph the shock is seen in two sequential positions as it approaches the end of the gage. The air to the right of the shock is undisturbed, while that to the left of (or behind) the shock is compressed and in motion toward the right. During the (approximate) 25 microseconds elapsed time between the two exposures the shock has advanced toward the gage from position 1 to position 2 at an average velocity of about 1470 feet per second. In the second photograph the shock is propagating across the leading edge of the gage. Thus in position 3 the shock front is located exactly at the leading edge of the gage, while (approximately) 25 microseconds later it has moved about 0.3 inch over the face of the gage. During this same time interval, a reflected shock has been formed at the leading edge of the gage and has propagated to the left, upstream against the afterflow of the main shock. The average velocity of the reflected shock is only 1032 feet per second as compared to 1472 feet per second for the incident shock in this case. The remaining two photographs show the shock as it propagates further along the gage, with the reflected wave becoming more nearly the arc of a circle as it propagates upstream.
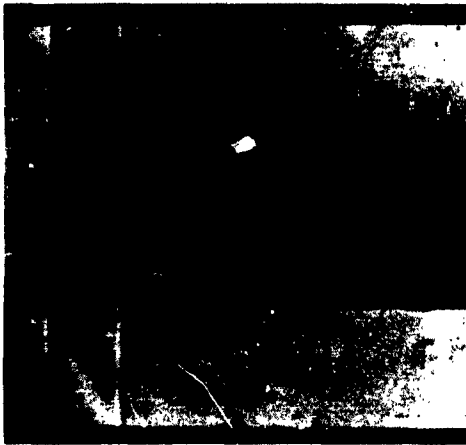
(A)
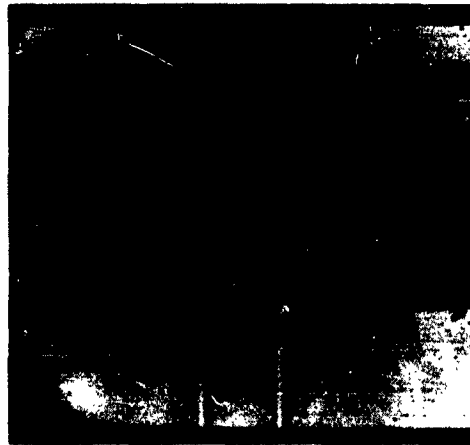
(B)

(C)

(D)

FIGURE 8: SHOCK TRAVELING OVER PILLBOX TYPE HOUSING. (BRL PHOTOGRAPH)

Figure 9 is a plot of the average velocity of the incident and reflected shocks as a function of position. At 12.5 psi peak pressures, at least, the average propagation velocity of a plane incident shock does not appear to change appreciably, less than 5 percent, as it encounters the BRL gage and propagates across the surface. The velocity of the reflected wave, however, decreases rapidly as it propagates upstream against the after-flow of the incident shock. This is probably caused, for the most part, by a decrease in shock intensity due to the spreading of the wave front.

Several other points of interest can be seen by closer examination of the photographs. To begin with, in corroboration of the fact that the curved trace is a reflected shock moving in a direction opposite to the incident shock, a change of phase of the optical density of the trace is noted. The dark line is on the downstream side of the incident shock and on the upstream side of the reflected shock, as is to be expected of shocks traveling in opposite directions in the same optical field. The lower density of the reflected wave image also means a lower shock intensity.

Another phenomenon is the development of a definite curvature to the shock front as it travels across the gage. The curvature is clearly evident in the last picture of Figure 8. A qualitative explanation of this can be evolved from the view that the mass of gas must be pushed aside as it flows across the gage housing, resulting in a sidewise compression. The resulting increase in pressure, greatest at the gage surface and decreasing outward, causes an increase in velocity, and the shock speeds up at the surface, thereby creating a curved shock front. Because of the pillbox shape of the BRL gage, the flow across the housing is actually three dimensional with much more curvature to the shock front than is evident at first.

Two other features of interest can also be seen on this last photograph of Figure 8. Immediately in front of the leading edge of the gage another weak shock can be seen. This is probably a detached shock formed by the quasi-steady subsonic flow following the main shock front in the shock tube. It is also interesting to note the rather fully developed turbulence at the top and bottom leading edges of the gage caused by this same after-flow. Both the curvature and the turbulence can also be seen in the preceding photograph.

A number of runs have also been made on a pancake type gage at 12.5 psi. No indications of reflections or turbulence are noticeable in the shadowgraphs of Figure 10. However, a definite curvature of the shock front develops as it

23
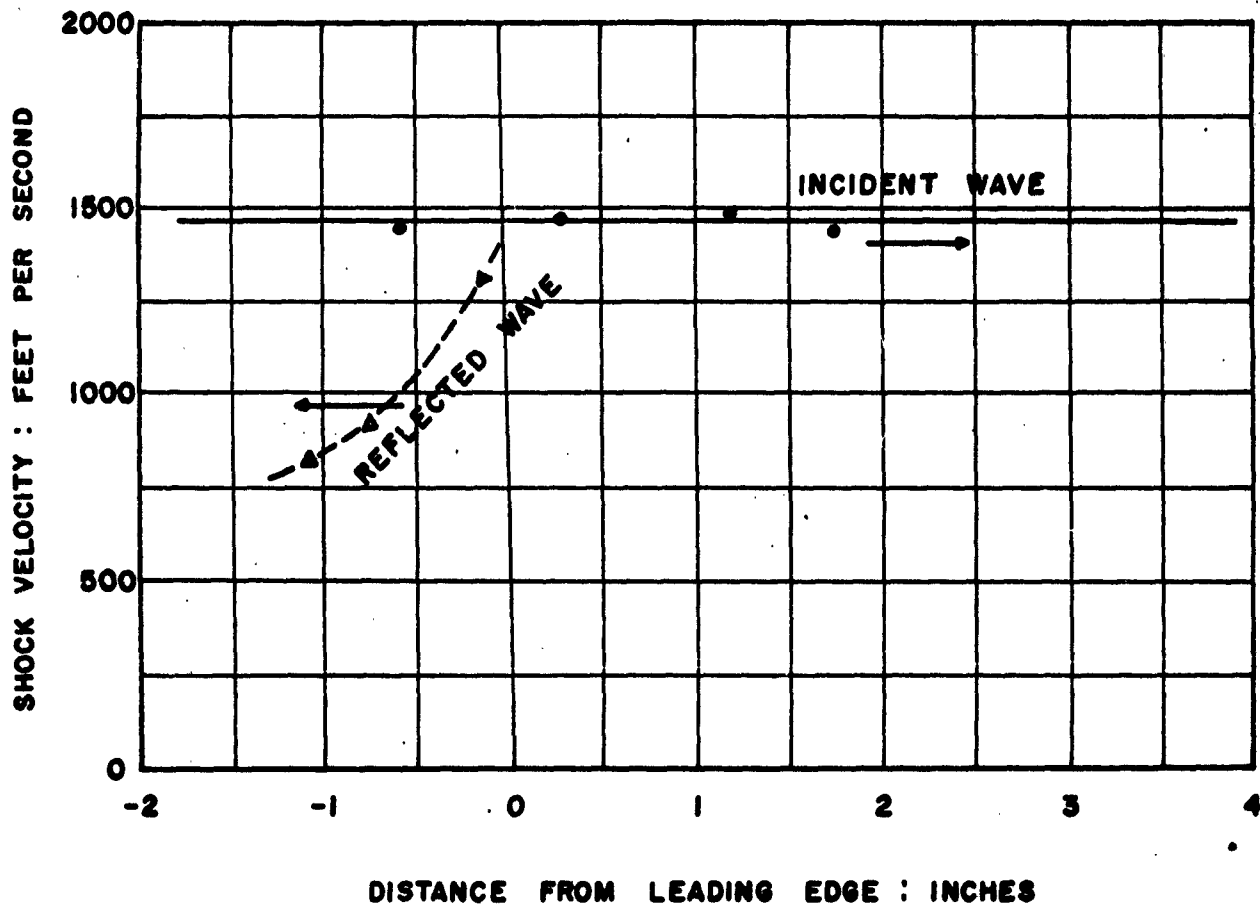
FIGURE 9 : SHOCK VELOCITY VS. POSITION
FOR PILLBOX TYPE HOUSING.

travels over the gage. This effect can be seen in the second and third pictures of Figure 10.

A similar set of tests was made in the shock tube at 12.5 psi with a streamlined gage of the pencil-type shown in Figure 6. No signs of reflections or turbulence are seen in the shadowgraphs of Figure 11. The shock travels over the gage with essentially no pertubation. Some curvature of the shock front develops near the gage surface as the shock passes over the nose of the gage, but this disappears by the time the shock reaches the position on the main cylindrical housing shown in Figure 11-c. Figure 12 shows that the shock velocity in the shock tube is not appreciably affected by passage over the gage.

The present shock tube studies have only been of a preliminary nature. It seems clear that an extended program of shock tube studies on blast gages, correlating shadowgraph, schlieren, or interferometer photographs with the recorded gage output, would go a long way toward a basic understanding of the air-blast transducer problem.

E. Field Investigation of the Effects of Gage Housing Shapes

Marks (17) has made field studies of errors in the observed peak pressure of air blast gages as affected by their housing shape. Pillbox, pancake, and pencil type gages were used with tourmaline discs as the sensitive element. One-pound bare spherical Pentolite charges were fired at a series of predetermined distances from the air blast gages to cover a peak pressure range of 10 to 80 psi. Both the charge and the gages were located in a free field high enough above the ground to avoid reflection. The peak pressure of the gage being tested was determined from the Rankine-Hugoniot equation, Equation (1), from measurements of average velocity made with a pair of time-of-arrival gages spanning each gage position. The outputs from the gages were displayed on an oscilloscope and recorded by a 35mm moving film camera. Although the effects of gage and amplifier frequency response are not always clearly separated from housing effects, Marks finds that large errors result from perturbations of the flow by the housings. The relative response of the gages as a function of peak pressure is shown in Figure 13. The pencil shaped housing is clearly superior to either the pancake or pillbox types.

(A)

(B)   (C)

FIGURE 10: SHOCK TRAVELING OVER PANCAKE
TYPE HOUSING. (BRL PHOTOGRAPH)

(A)

(B)

(C)

(D)
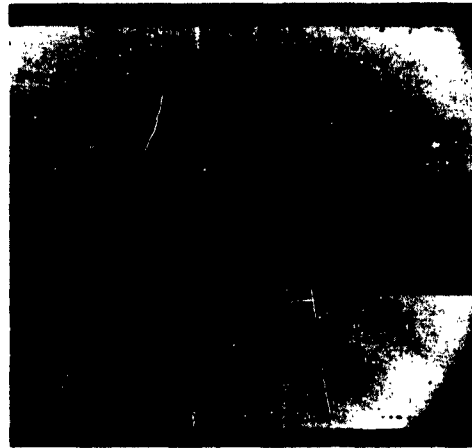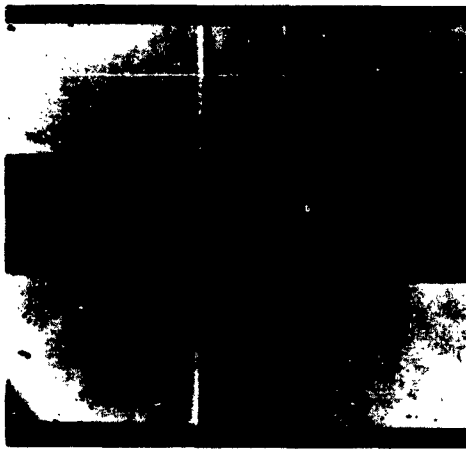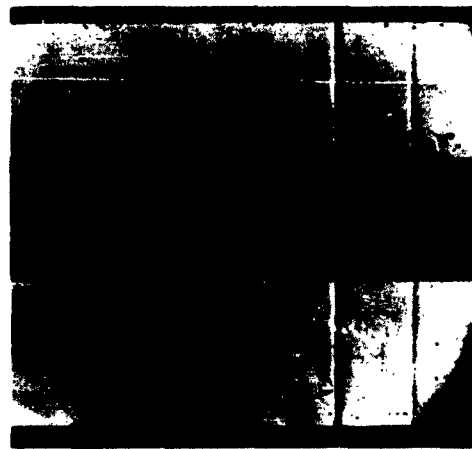
FIGURE II :   SHOCK   TRAVELING   OVER   PENCIL
                TYPE   HOUSING. (BRL PHOTOGRAPH)
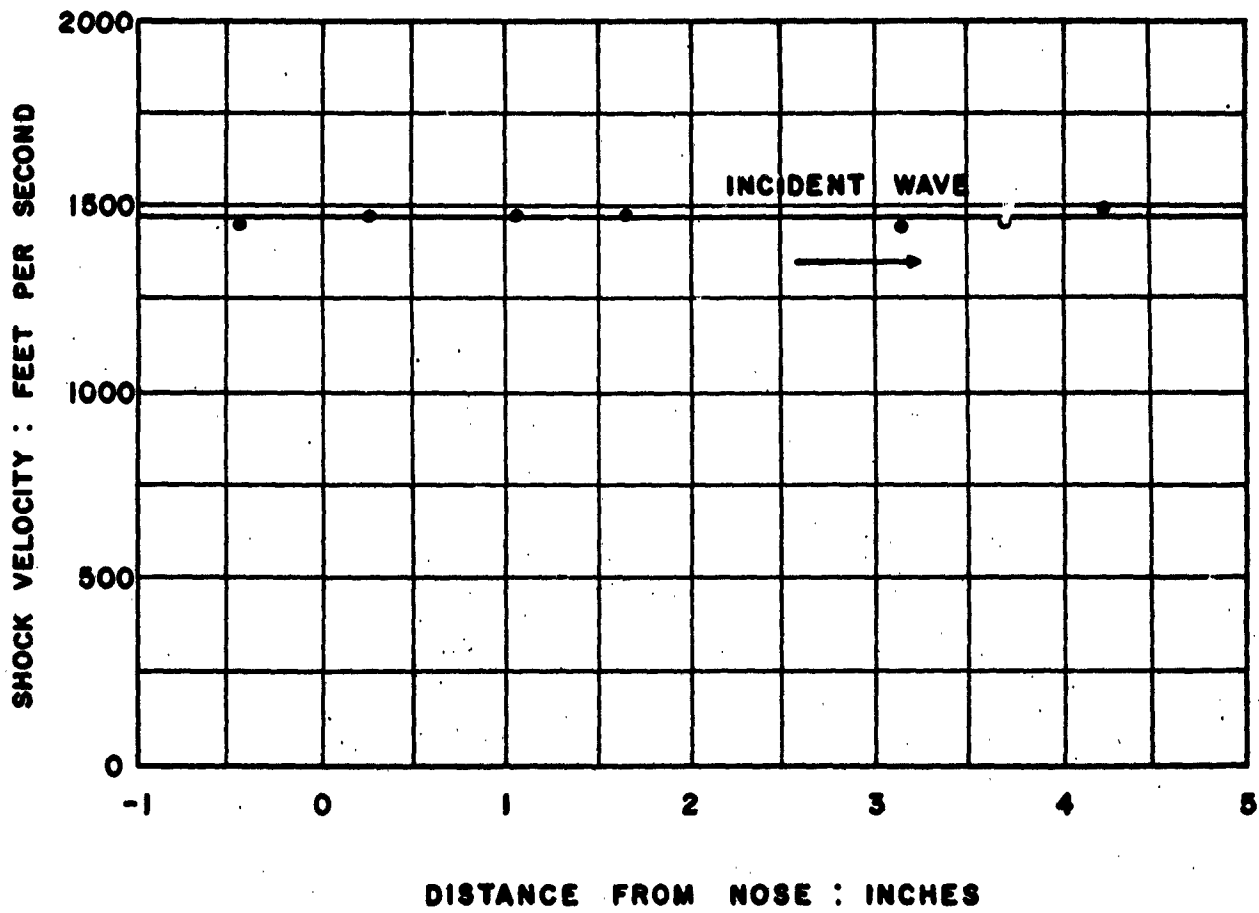
FIGURE 12: SHOCK VELOCITY VS. POSITION
FOR PENCIL TYPE HOUSING.
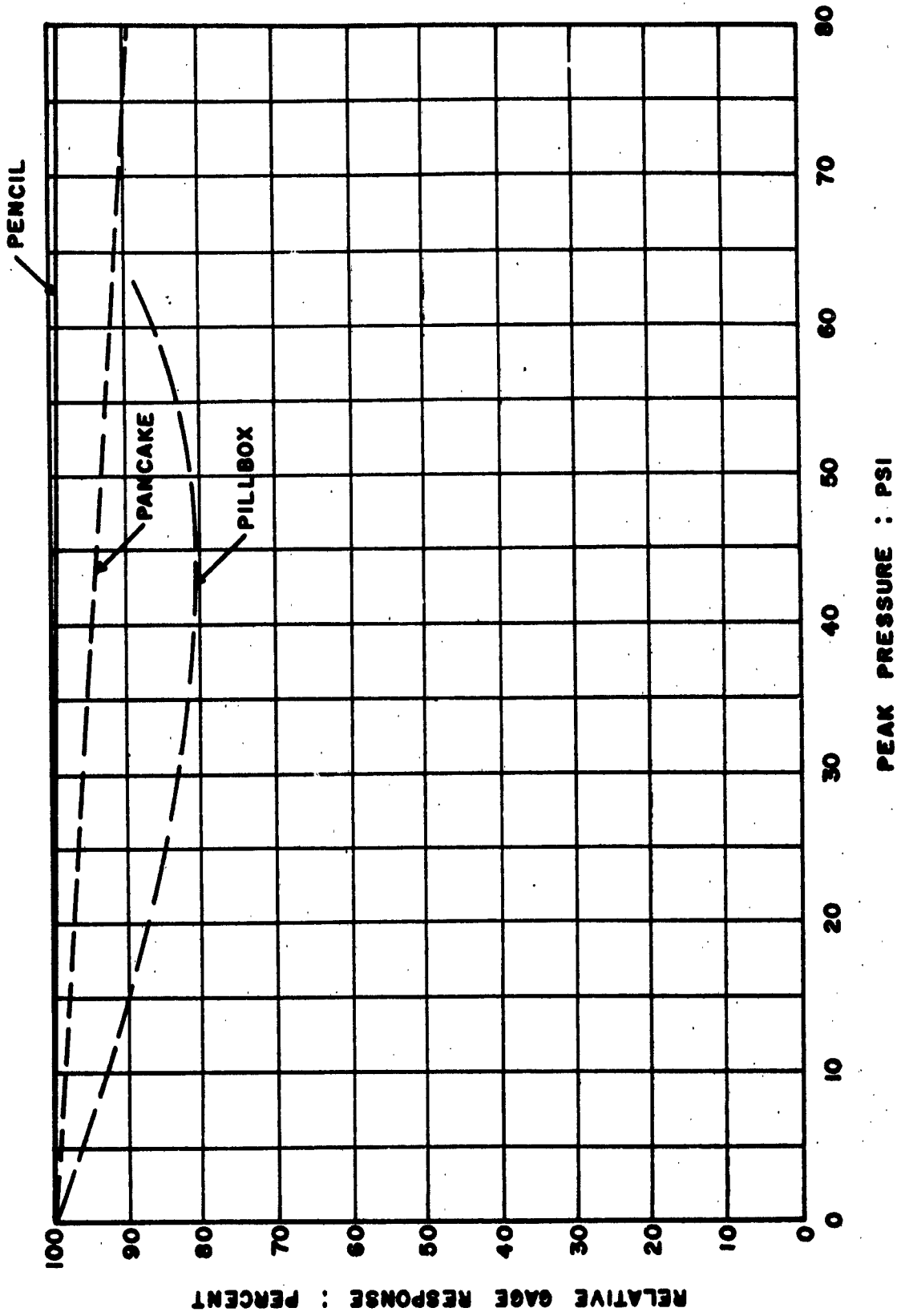
FIGURE 13 : RELATIVE RESPONSE VS. PEAK PRESSURE FOR VARIOUS GAGE SHAPES. (AFTER MARKS)

Measurements of this kind are important and should be extended to include shadowgraphs of the shock passing over the gage in the free field. Future investigations should include a study of the effects of the shock traveling across the gage at various angles. Comparisons should be made with various housings, using sensitive elements of identical electroacoustic characteristics, i.e., impedance, sensitivity, frequency response, etc. The correlation of such investigations with shock-tube measurement would be of considerable interest.

III. ELECTROACOUSTIC PROPERTIES OF BARIUM TITANATE CYLINDERS

Having established the aerodynamic superiority of pencil shaped streamlined housings for air blast gages, attention is now directed to the problem of incorporating a sensitive element into the housing for the purpose of converting the transient shock pressure into a corresponding electrical signal. Although a variety of transducer mechanisms have been used for blast measurements, it can be stated that piezoelectric systems, adequately designed and properly used, are superior for the purpose. Of the known piezoelectric materials barium titanate in the form of a tube or cylinder lends itself most readily for use in the pencil gage. The electroacoustical properties of such elements will be reviewed with regard to their application to air blast gages.

A. General Design Considerations

This phase of the problem resolves itself into a one-dimensional study of the transient response of an electroacoustical element. Although the problem is essentially a matter of the transient response of a system, the technique of Laplace transforms (18) allows the problem to be considered from a steady state standpoint. The faithful reproduction of the discontinuous rise and rapid decay of shock wave pressure carries with it the requirement of sufficiently faithful response at high frequency so that the peak will not be rounded off appreciably.

The low frequency requirements present a similar problem and become important when the impulse or integral under the pressure-time curve is desired. Cole (19) has made an analysis of the case for the problem of amplifier circuits associated with blast measurements, and the problem of the transducer

is the same. He obtains the following equations for the relative transient response to an exponentially decaying pulse:

High frequency cut-off:

$$R(t) = \frac{P_o}{1 - \frac{T}{\theta}} \left[e^{-\frac{t}{\theta}} - e^{-\frac{t}{T}} \right] \qquad (5)$$

Low frequency cut-off:

$$R(t) = \frac{P_o e^{-\frac{t}{\theta}}}{1 - \frac{\theta}{\lambda}} \left[1 - \frac{\theta}{\lambda} e^{(1 - \frac{\theta}{\lambda})\frac{t}{\theta}} \right] \qquad (6)$$

The symbols used above are defined as follows:

$R(t)$ is the relative response, a function of time t;

P_o is the amplitude of the pulse;

θ is the pulse decay constant;

T is the high-frequency time constant;

λ is the low-frequency time constant; and

e is the base of natural logarithms.

These expressions plotted as a function of $\frac{t}{\theta}$ are shown in Figures 14 and 15. Note, from Figure 15, that an apparent negative pulse will be observed if the low-frequency response is not adequate.

The problem from a transducer standpoint becomes then a matter of designing a unit that has a flat frequency response from frequency f_1, determined by the requirements for low-frequency response, to frequency f_2, determined by the requirements for high-frequency response. With piezo-electric materials such as barium titanate, this becomes a matter of designing the vibrating element so that it is "stiffness controlled," the lowest fundamental mode of vibration being well above the highest frequency of interest. At the other end of the frequency spectrum, the low-frequency cut-off is determined essentially by the RC time constant of the transducer. This becomes a combined problem of designing for as high a capacitance and as high a leakage resistance as possible for the transducing element. The low-frequency cut-off is, of course, affected by the load resistance of the associated amplifier in the recording circuit. The amplifier must ordinarily be designed for a high input resistance.
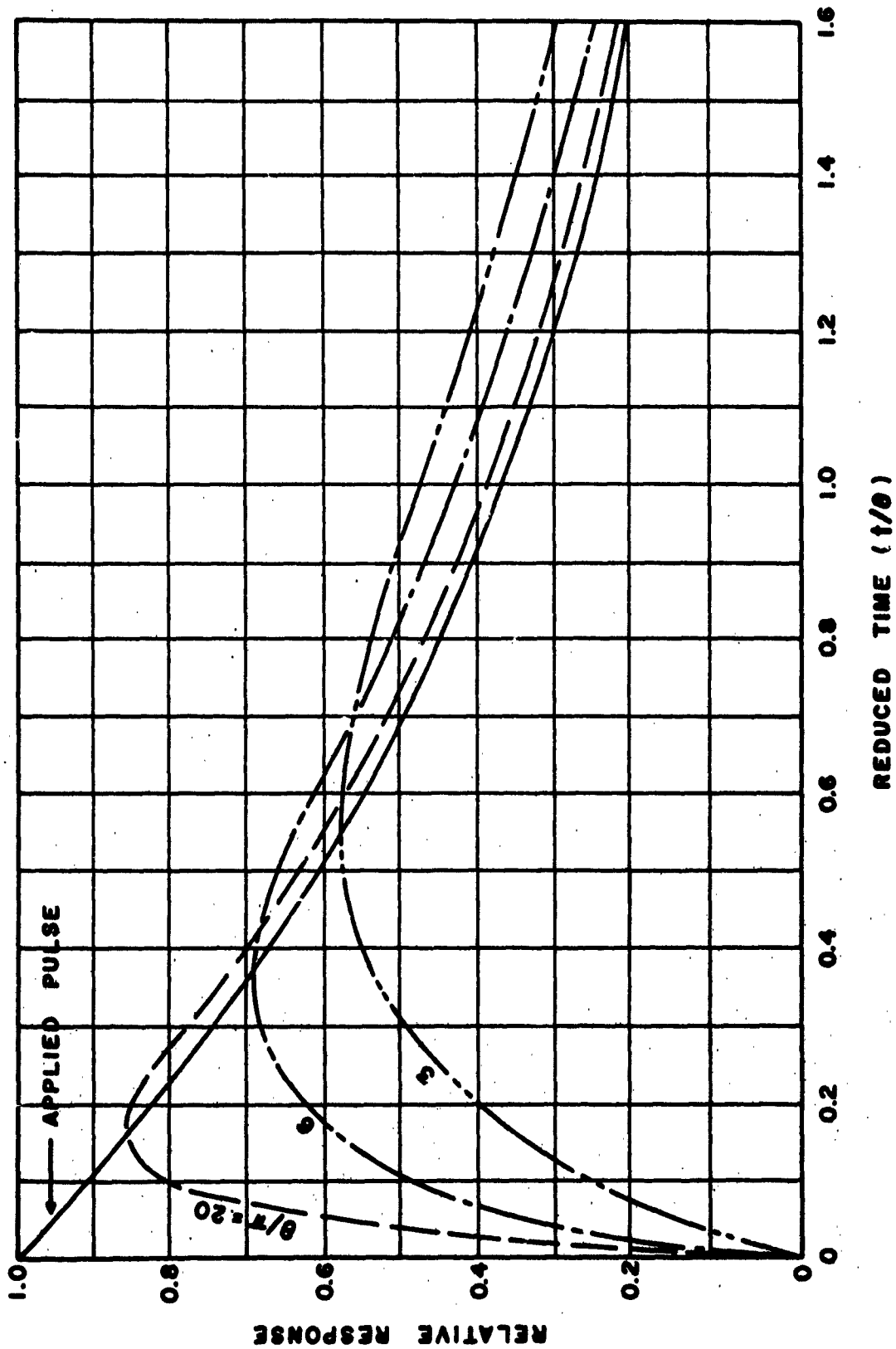
FIGURE 14 : RELATIVE ERROR DUE TO HIGH FREQUENCY
CUT-OFF. (AFTER COLE)

32
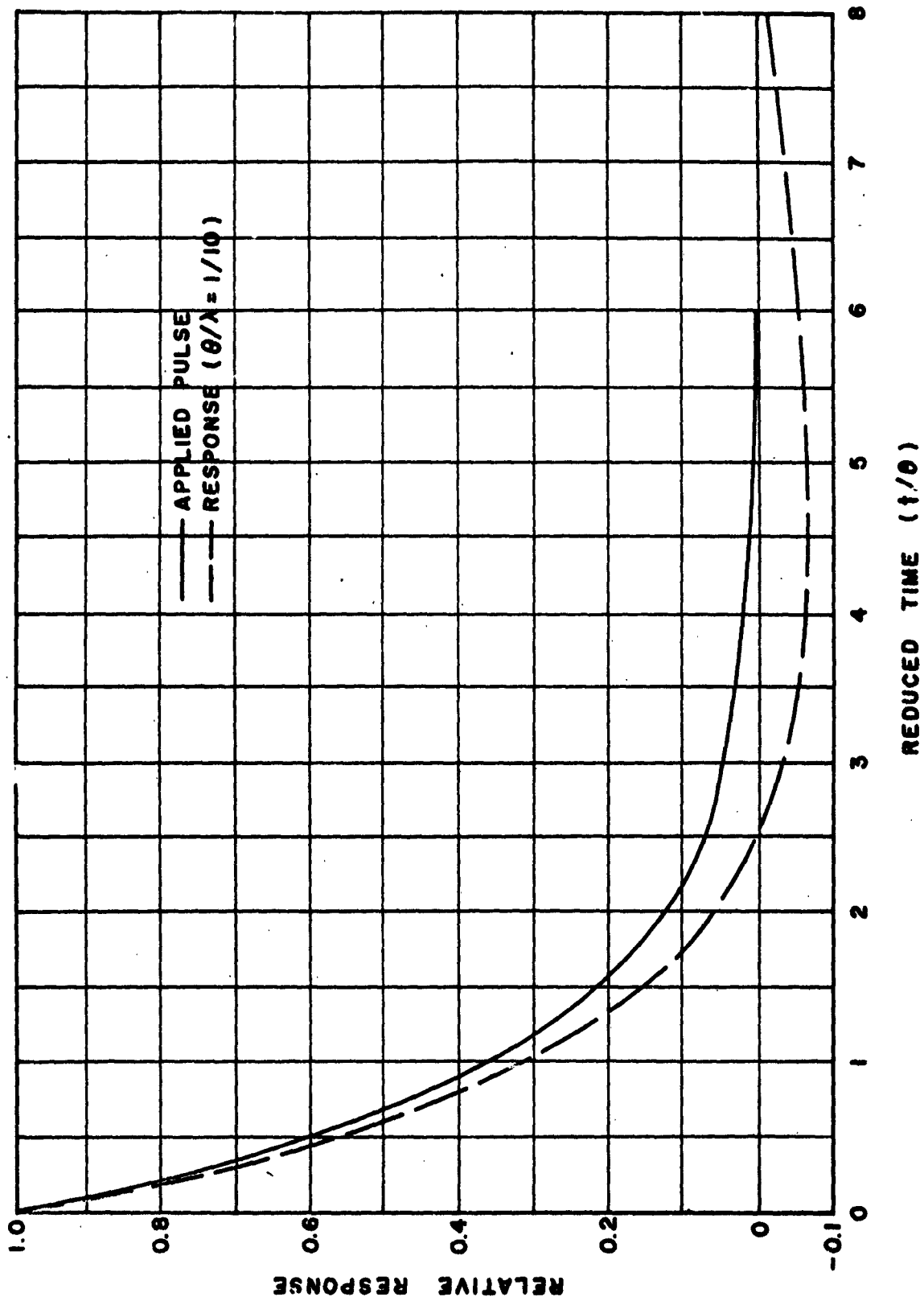
FIGURE 15 : RELATIVE ERROR DUE TO LOW · FREQUENCY
CUT-OFF. (AFTER COLE)

33

B. Review of Piezoelectric Constants (20)

From a phenomenological viewpoint, barium titanate can be treated as a piezoelectric material although it is classed as a ferroelectric material. In order to describe its behavior as a transducer, the external variables of stress, strain, field, and charge must be considered together with the intrinsic properties of the material, viz., the elastic constants, dielectric constants, density, and piezoelectric constants.

Of the constants, the density is independent of the shape of the piece or mode of vibration. As a first approximation, barium titanate can be considered as isotropic insofar as the elastic constants are concerned, so that the ordinary Young's modulus, Poisson's ratio, rigidity modulus, etc., can be used with no dependence on direction. The same consideration applies to the dielectric constant. This is not the case, however, for the piezoelectric constants. Their values depend on the relative direction between the stress and the polarization. This can be clarified for simple bodies by reference to Figure 16. For the bar, the length L is along the axis (1), and width w along axis (2), and the thickness t along axis (3). The disc of radius a is oriented in the plane of axis (1) and (2) with the thickness t along axis (3). For the cylinder, cylindrical coordinates (r, θ, Z) are used, with length of the cylinder L along axis (1). For an infinitesimal section of cylinder, the same orientation in cartesian coordinates can be assumed as shown. All elements are assumed to have metallic electrodes on the surfaces perpendicular to the (3)-axis and to have been polarized along this axis. This applies to the cylinder since the (3)-axis is coincident with the (r)-axis. If an AC voltage is applied to the electrodes modal vibrations are excited as follows:

For the Bar:

(1) Expansion and contraction along axis (1), the bar length mode, characterized by the indices (3,1) since the electric-field is in the (3)-direction and the mechanical strain in the (1)-direction;

(2) Expansion and contraction along the (3)-axis, the bar thickness mode, characterized by the indices (3,3); and

a. PIEZOELECTRIC BAR.
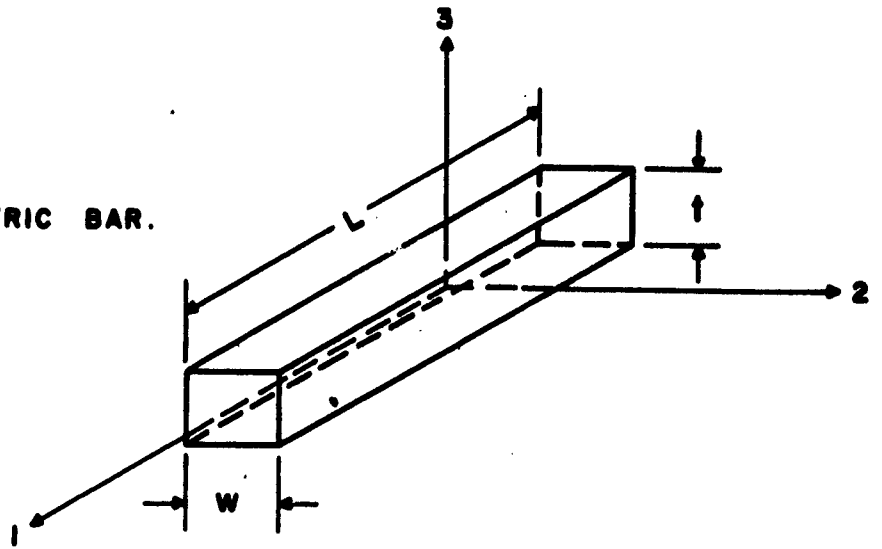
b. PIEZOELECTRIC DISC.
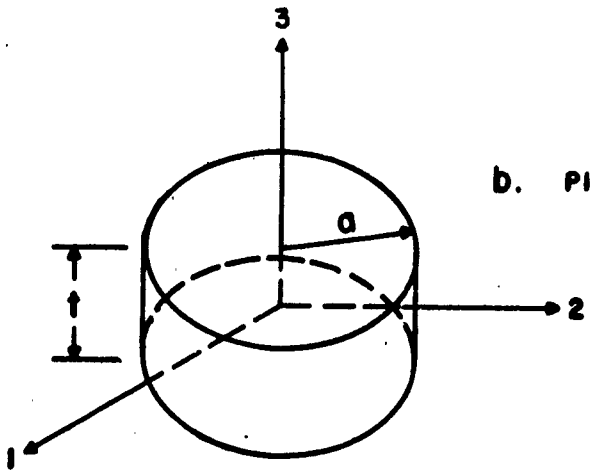
c. PIEZOELECTRIC CYLINDER.
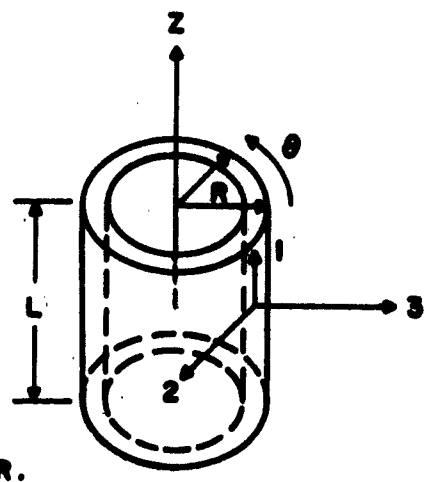
FIGURE 16 : SIMPLE PIEZOELECTRIC ELEMENTS.

(3) Expansion and contraction along axis (2), a direction assumed
to have the same properties as axis (1) for barium titanates.
For a bar with $\frac{W}{L} \ll 1$, motion along the (2)-axis is negligible.

For the Disc:

(1) Expansion and contraction in the direction of the radius, called
the disc radial mode, and characterized by the indices (3,1); and

(2) Expansion and contraction along axis (3), the disc thickness mode,
and characterized by the indices (3,3).

For the Cylinder:

(1) Expansion and contraction along the (1)-axis, called the length
mode, and characterized by the indices (3,1);

(2) Expansion and contraction along the radius or (3)-axis, called
the thickness mode, and characterized by the indices (3,3); and

(3) Expansion and contraction along the circumference or (2)-axis,
called the circumferential mode, and, since for barium titanate
the properties of the (1) and (2) axis are assumed the same,
characterized by the indices (3,1).

The meaning of the piezoelectric constants, the so-called d- and
g-constants, can be illustrated with a simple example. If a pressure p is
applied to the disc in the direction of the (3)-axis, the charge density q
appearing on the electrode is given by:

$$q = d_{33} \cdot p \qquad (7)$$

where d_{33} is the piezoelectric (charge) coefficient. Multiplying the fore-
going by the area A of the electrodes gives $A \cdot q = d_{33} \cdot p \cdot A$ or

$$Q = d_{33} \cdot F \qquad (8)$$

where Q is the total charge and F is the total load. If, on the other hand,
we apply an electric field E in the same direction the resulting strain

$$s = d_{33} \cdot E \qquad (9)$$

and multiplying by the thickness t gives $st = d_{33}E \cdot t$ or

$$S = d_{33} \cdot V \qquad (10)$$

where S is the total change in thickness and V is the applied voltage.

The voltage resulting from an applied force is obtained from Equation (8) by noting that $Q = C \cdot V$ where C is the capacitance of the disc. Hence, since $C = \frac{\epsilon A}{t}$ where ϵ is the dielectric constant,

$$V = \frac{Q}{C} = \frac{d_{33} \cdot F}{C} = \frac{d_{33}}{\epsilon} \cdot \frac{F}{A} \cdot t; \tag{11}$$

or dividing by t,

$$E = g_{33} \cdot P, \tag{12}$$

where the $g_{33} = \frac{d_{33}}{\epsilon}$. Similarly

$$s = g_{33} \cdot q . \tag{13}$$

The other piezoelectric constants d_{31} and g_{31} can be described in a like manner except that the electrical and the mechanical effects are in different planes.

Titanates are also sensitive to hydrostatic pressure and the so-called volume-expander constants are related to the foregoing piezoelectric constants as follows:

$$d_h = d_{33} + 2d_{31}$$

$$g_h = g_{33} + 2g_{31} \tag{14}$$

In addition, barium titanate also has shear piezoelectric constants characterized by d_{15} and g_{15}, but these are ordinarily of no interest in the design of transducers for air blast measurements.

An important parameter of piezoelectric materials is the electro-mechanical coupling coefficient, k (21). It is the best single figure-of-merit of a transducer and is defined as the square root of the ratio of the electrical energy output to the mechanical energy input. It can be shown to be a function of the piezoelectric coefficient and the particular stress function applicable to a given sample shape and loading condition. It is also related to the absolute efficiency and, hence, to self noise. For the simple thickness mode, the coupling coefficient k is given by

$$k = d_{33} \sqrt{\frac{Y}{\epsilon}} \tag{15}$$

where Y is Young's Modulus and ϵ is the dielectric constant. For the bar length mode and radial disc mode the corresponding equations are, respectively,

$$k = d_{31} \sqrt{\frac{Y}{\epsilon}} \qquad (16)$$

$$k = d_{31} \sqrt{\frac{Y}{\epsilon} \cdot \frac{2}{1-\sigma}} \qquad (17)$$

where σ is Poisson's ration and the other symbols are defined above. The value for a cylindrical barium titanate element is somewhat more complicated and can be shown (22) to be of the form

$$k^2 = \frac{b^2 \left[g_{33}(\frac{a-b}{a+b}) - g_{31} \right]^2 \times \frac{0.6128\ \epsilon}{\log\ (b/a)}}{b^2 \left[g_{33}(\frac{a-b}{a+b}) - g_{31} \right]^2 \times \frac{0.6128\ \epsilon}{\log\ (b/a)} + \frac{2\pi l b^2}{Y} \left| \sigma - \frac{b^2 + a^2}{b^2 - a^2} \right|} \qquad (18)$$

Here, the inside diameter of the cylinder is 2a, the outside diameter is 2b, the length is l, and the other symbols have been previously defined.

C. Summary Properties of the Titanates

The properties of barium titanate ceramic materials have been treated elsewhere (23, 24, 25, 26). For reference purposes, the piezoelectric constant, and coupling coefficient are given below in Table I for barium titanate with 5% calcium titanate added, and tourmaline. The barium titanate with 5% calcium titanate was used in the air blast gages constructed during this project (1, 2, 3).

TABLE I

Selected Properties of Certain Piezoelectric Materials

Material	d_{33} Piezoelectric Coefficient (Coulombs per Newton)	Relative Dielectric Constant	Coupling Coefficient (percent)
Barium Titanate	190×10^{-12}	1700	50
Barium Titanate with 5% Calcium Titanate	140×10^{-12}	1200	46
Tourmaline	1.9×10^{-12}	6.6	10

Many of the properties of the titanates are temperature dependent. This dependence is illustrated in Figures 17 through 19 which show the variation of the dielectric constant, the electromechanical coupling coefficient, and the piezoelectric coefficient with temperature for a number of titanate compositions.
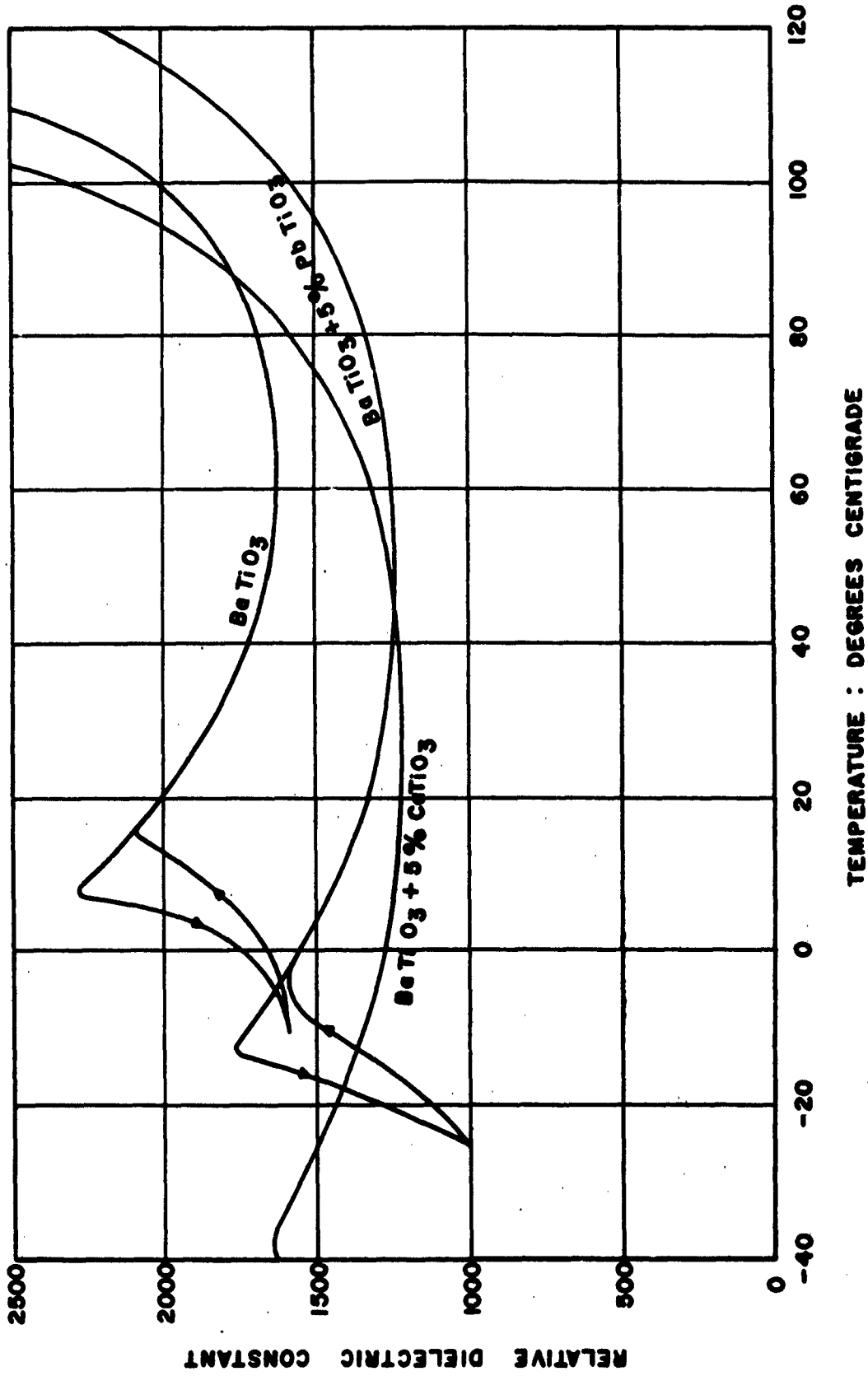
FIGURE 17 : DIELECTRIC CONSTANT VS. TEMPERATURE.

(AFTER MASON)

39
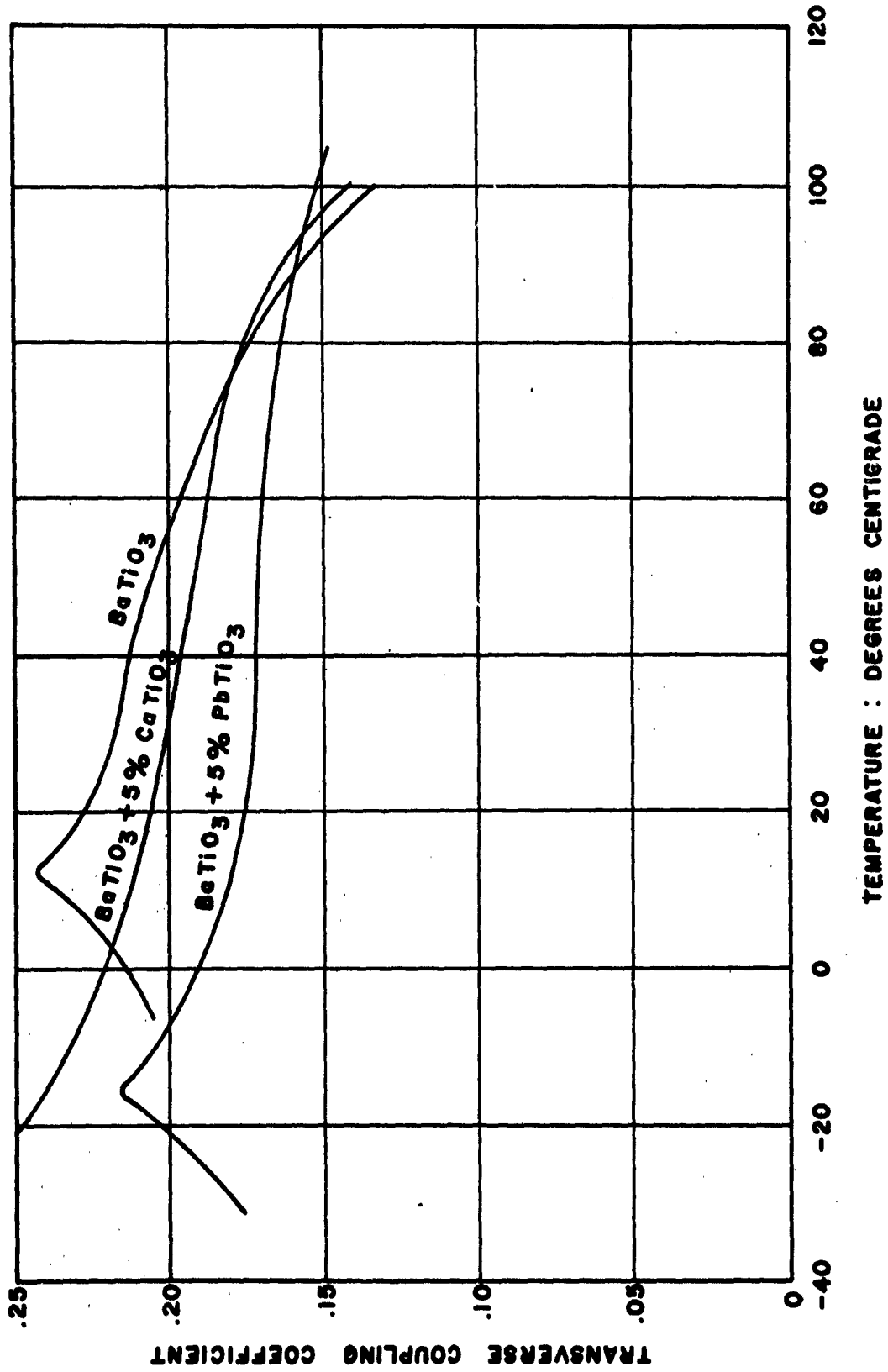
FIGURE 18: ELECTROMECHANICAL COUPLING COEFFICIENT VS. TEMPERATURE. (AFTER BERLINCOURT)

40
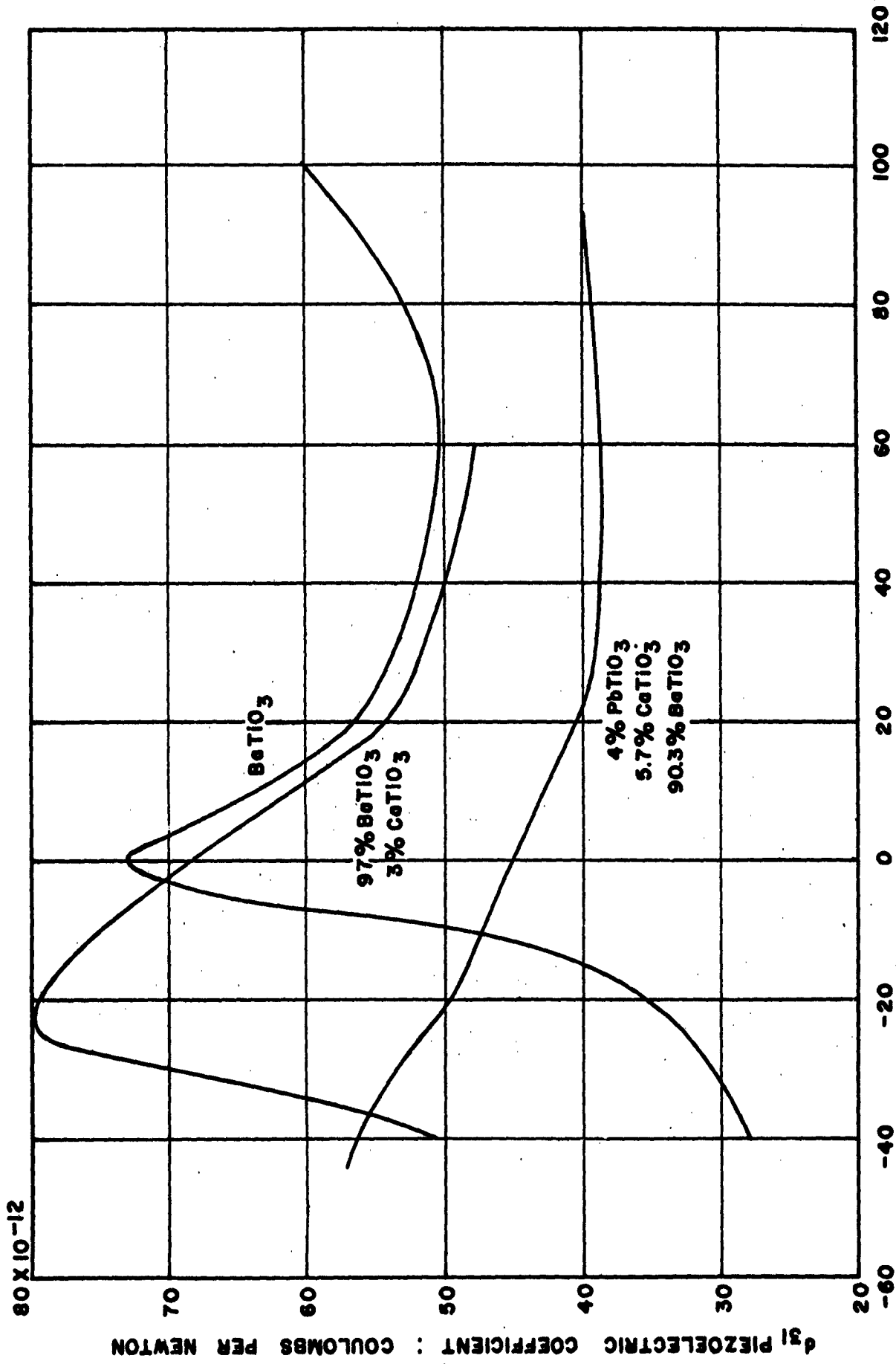
FIGURE 19 : VARIATION OF PIEZOELECTRIC COEFFICIENT
WITH TEMPERATURE. (AFTER MASON)
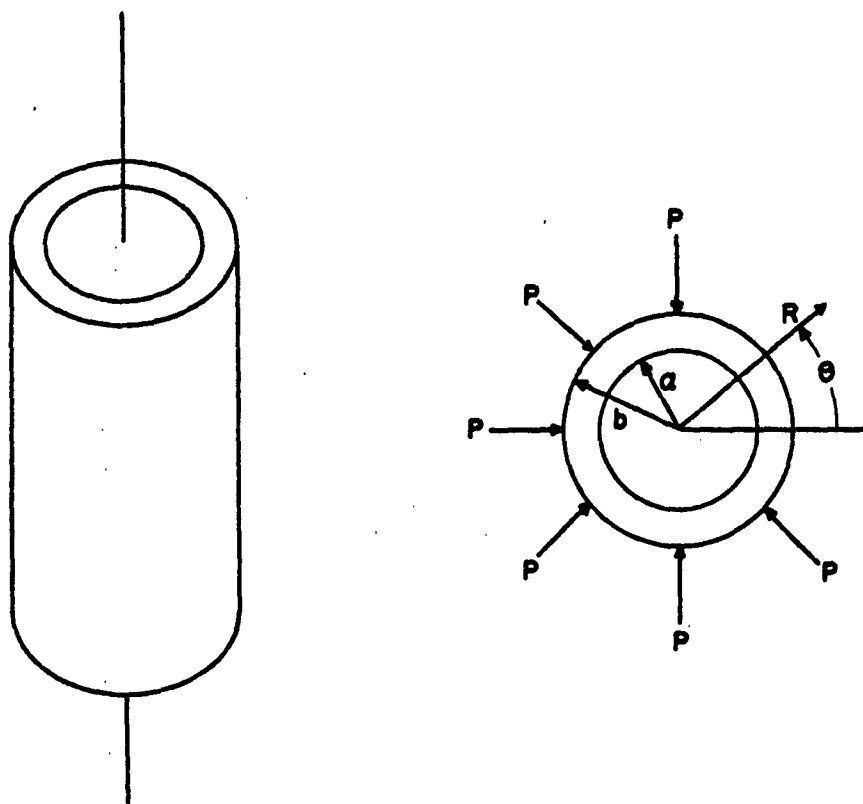
FIGURE 20: EXTERNALLY LOADED BARIUM TITANATE CYLINDER.
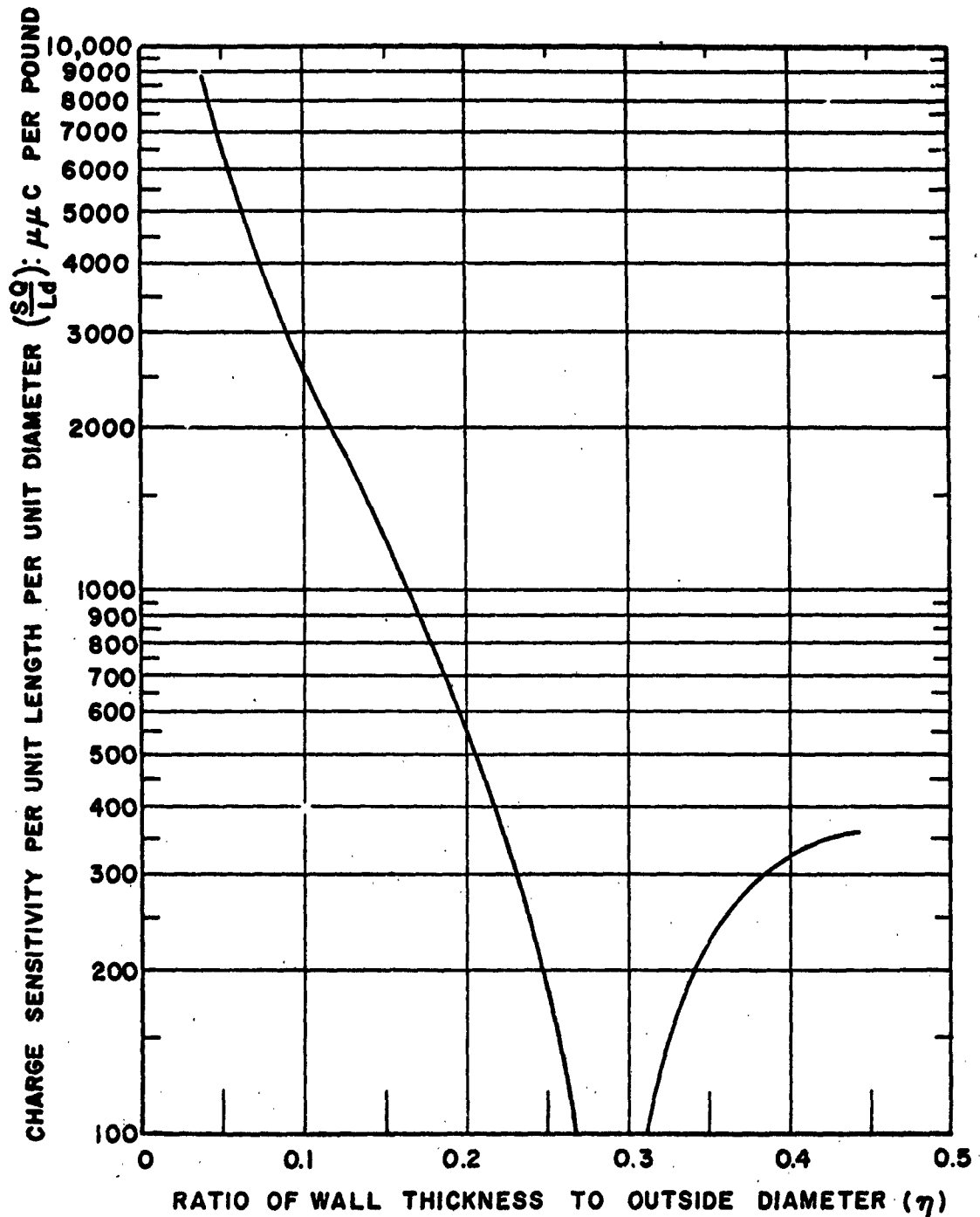
FIGURE 21 : CHARGE SENSITIVITY OF A CYLINDER AS A FUNCTION OF THE RATIO OF WALL THICKNESS TO OUTSIDE DIAMETER; A PLOT OF EQUATION (27) FOR BARIUM TITANATE WITH 5 % CALCIUM TITANATE ADDITIVE.
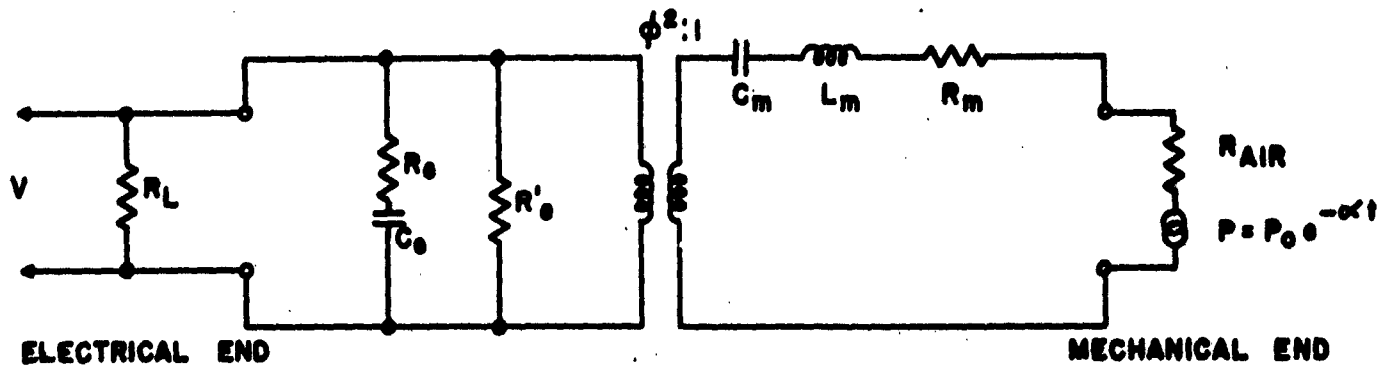
a. COMPLETE EQUIVALENT CIRCUIT
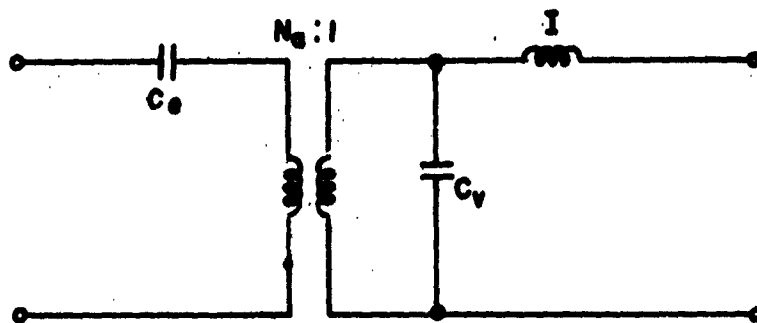
b. SIMPLIFIED EQUIVALENT CIRCUIT

FIGURE 22: EQUIVALENT CIRCUITS FOR CYLINDRICAL
TUBES OF BARIUM TITANATE. (REF. 22)
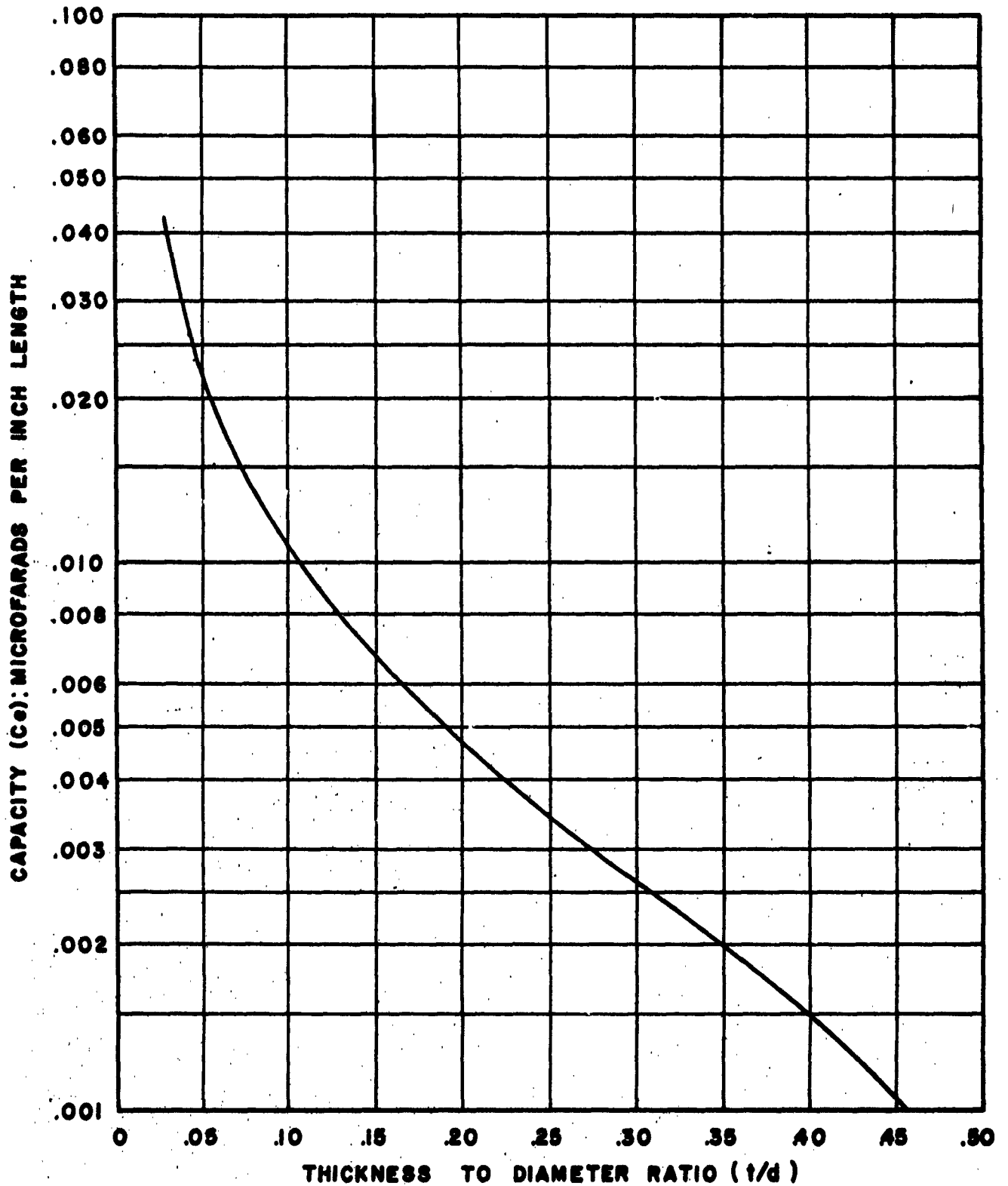
FIGURE 23 · CAPACITANCE VS. RATIO OF THICKNESS
TO DIAMETER FOR CYLINDRICAL TUBES
OF BARIUM TITANATE. (REF. 22)

45
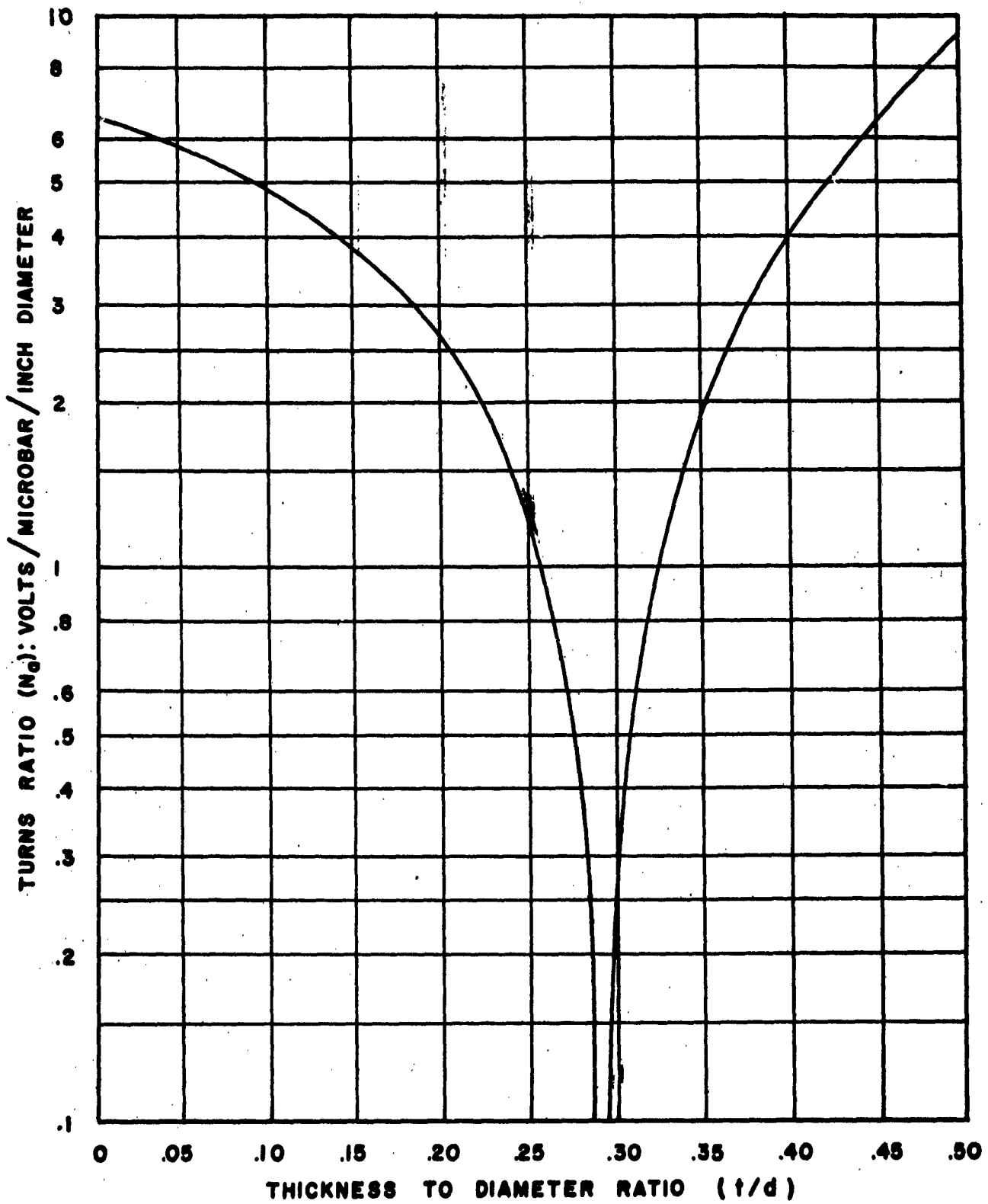
FIGURE 24 : TURNS RATIO VS. RATIO OF THICKNESS TO DIAMETER FOR CYLINDRICAL TUBES OF BARIUM TITANATE. (REF. 22)
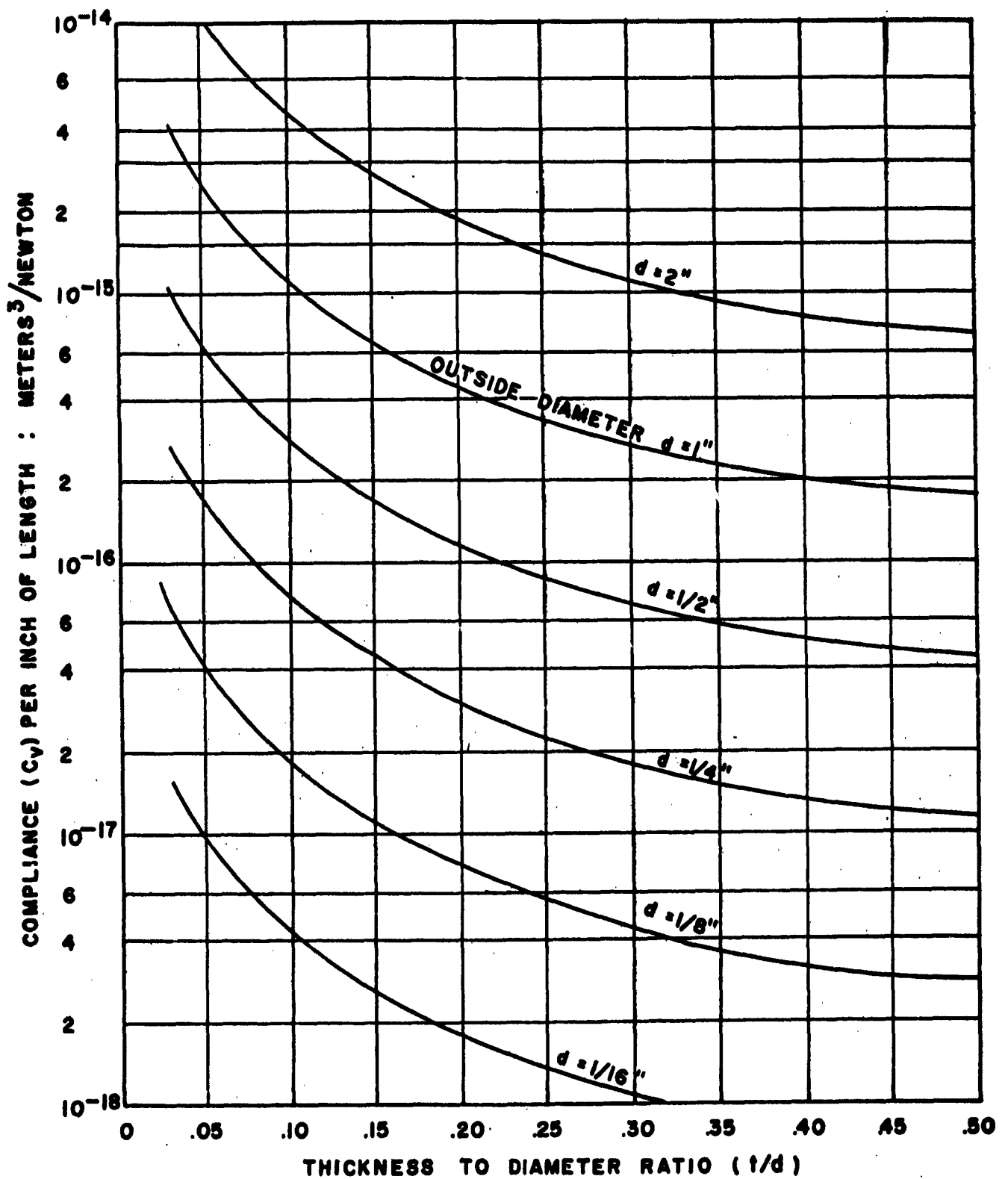
FIGURE 25 : MECHANICAL COMPLIANCE VS. RATIO OF
THICKNESS TO DIAMETER FOR CYLINDRICAL
TUBES OF BARIUM TITANATE. (REF. 22)
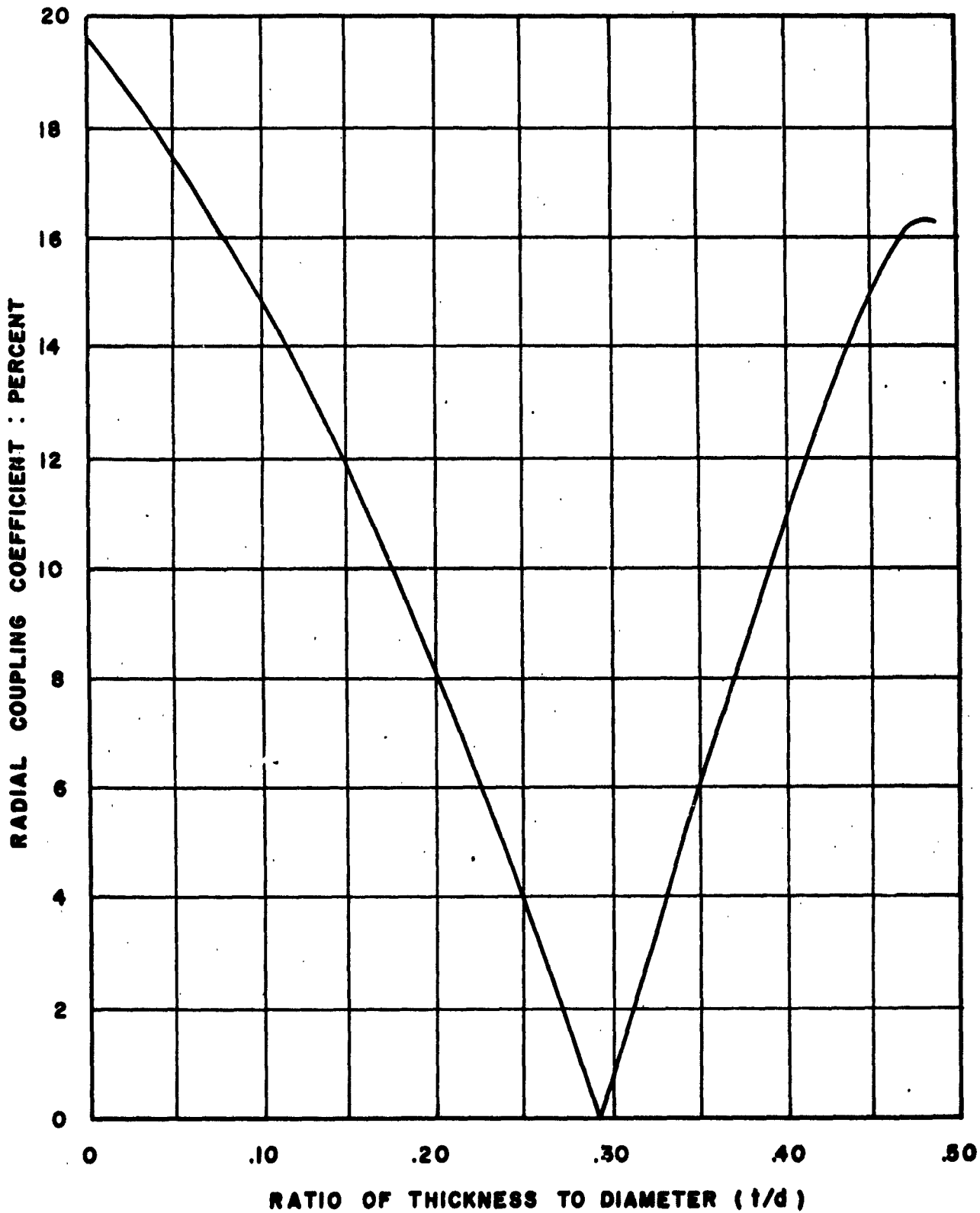
FIGURE 26 : COUPLING COEFFICIENT VS. RATIO OF THICKNESS
TO DIAMETER FOR CYLINDRICAL TUBES OF
BARIUM TITANATE, (REF. 22)
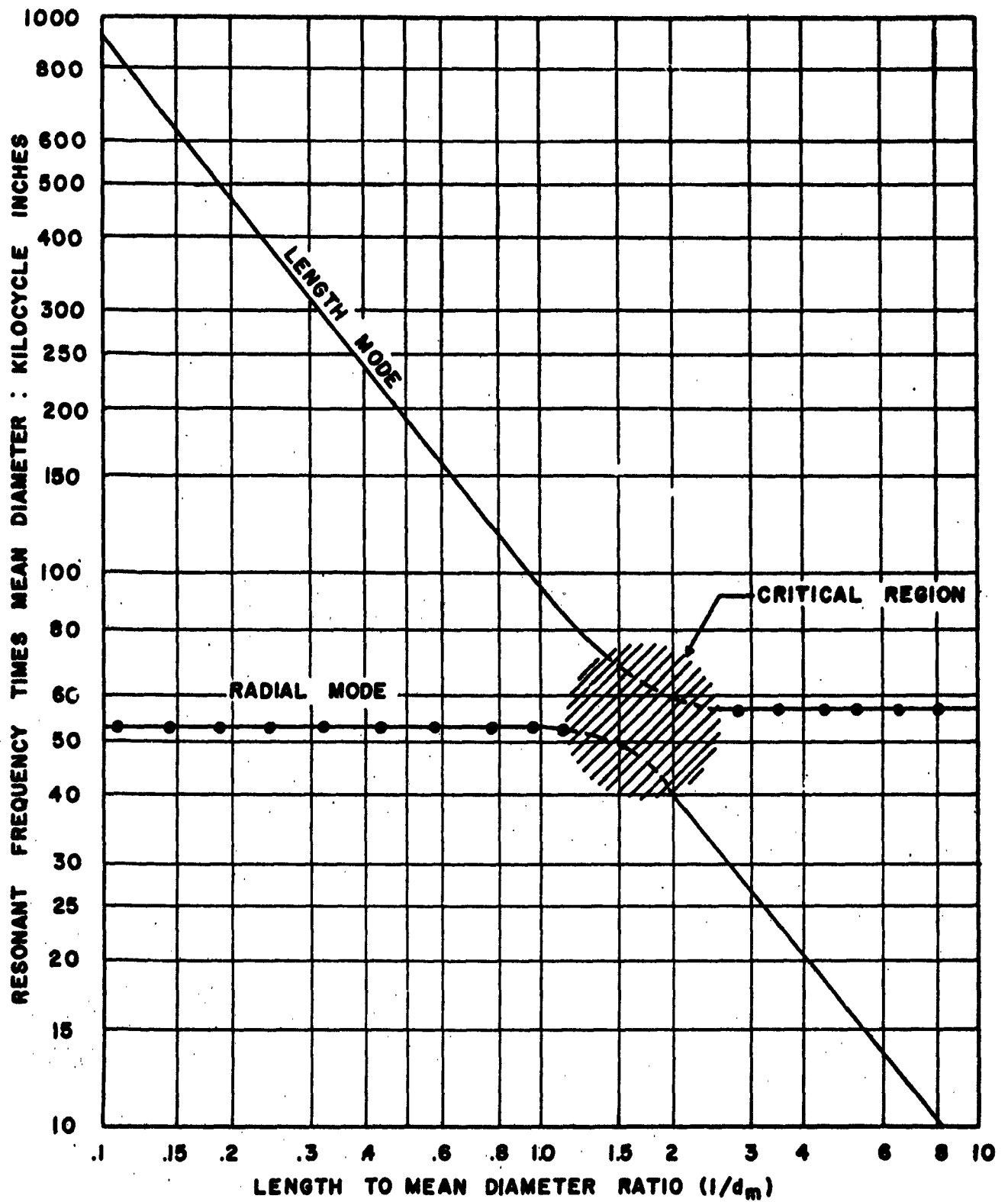
FIGURE 27 : RESONANT FREQUENCY VS. RATIO OF LENGTH TO MEAN DIAMETER FOR CYLINDRICAL TUBES OF BARIUM TITANATE. (REF. 22)

Since air blast measurements may have to be made at temperatures from somewhat below zero to +30°C or so, the effects of temperature on the electroacoustical characteristics of titanate are important.

The phenomenon of pyroelectricity is a complicated one and arises from changes in polarization charges with a change of temperature. The effect in barium titanate can be particularly distressing since thermal effects due to the compressive heating of the shock wave can result in large errors in the measurement of pressure. With proper design, thermal insulation can minimize the pyroelectric effects without seriously affecting pressure response.

D. Elementary Theory of Cylindrical Transducer

For frequencies well below the lowest resonance, the sensitivities of cylindrical barium titanate shells for various boundary conditions and polarizations have been calculated by Langevin (27). In this range, the response is "stiffness controlled" and the stresses determined from elastic theory can be used, with the piezoelectric constants, to calculate the sensitivity. Following Langevin, and referring to Figure 20, it can be shown that the stresses for uniform pressure P on the outside of the cylinder are

$$T_R = \frac{a^2 b^2 P}{b^2 - a^2} \left\{ \frac{1}{R^2} - \frac{1}{a^2} \right\} \tag{19}$$

$$T_\theta = \frac{a^2 b^2 P}{b^2 - a^2} \left\{ -\frac{1}{R^2} - \frac{1}{a^2} \right\} \tag{20}$$

$$T_z = 0, \tag{21}$$

where T_R, T_θ, T_z are the components of stress in the radial, circumferential, and axial directions, respectively. For an element of volume with edges dR, $Rd\theta$, and d_z the stresses T_R, T_θ, and T_z will produce electric fields E_R (radial), E_θ (circumferential), and E_z (axial) as follows:

$$E_R = g_{33} T_R$$

$$E_\theta = g_{32} T_\theta \tag{22}$$

$$E_z = g_{31} T_z = 0$$

The total voltage V developed between the inner and outer surfaces of the cylinder will be simply

$$V = \int_a^b \left[g_{33} T_R + g_{31} T_\theta \right] dR \qquad (23)$$

which gives, upon integration and rearrangement,

$$S_V = \frac{V}{P} = b \left[g_{33} \left(\frac{\rho-1}{\rho+1} \right) - g_{31} \right] \qquad (24)$$

where S_V is the voltage sensitivity and ρ is written for the ratio a/b.

Since $Q = V \times C$, the charge sensitivity S_q is simply

$$S_q = \frac{Q}{P} = cb \left[g_{33} \left(\frac{\rho-1}{\rho+1} \right) - g_{31} \right] . \qquad (25)$$

If L is the length of the cylinder (assumed to be long), its capacitance is given by $C = \frac{2\pi\epsilon L}{\ln(1/\rho)}$, so that the charge sensitivity becomes

$$S_q = \frac{2\pi\epsilon Lb}{\ln(1/\rho)} \left[g_{33} \left(\frac{\rho-1}{\rho+1} \right) - g_{31} \right] . \qquad (26)$$

Using the parameter $\eta = t/d$, the ratio of the wall thickness t to the outer diameter d, Equation (26) can be reduced to the convenient form

$$\frac{S_q}{L_d} = \frac{\pi}{\ln \left(\frac{1}{1-2\eta} \right)} \times \left[d_{33} \left(\frac{-\eta}{1-\eta} \right) - d_{31} \right] . \qquad (27)$$

Figure 21 shows the form of Equation (27), with neglect of the change in sign which occurs at about $\eta = 0.285$, based on the following constants for barium titanate with 5% of calcium titanate added:

$$d_{33} = 140 \times 10^{-12} \text{ coulomb/meter}^2 // \text{Newton/meter}^2 \qquad (28)$$

$$d_{31} = -56 \times 10^{-12} \text{ coulomb/meter}^2 // \text{Newton/meter}^2 \qquad (29)$$

It is interesting to note that the sensitivity is extremely low in the vicinity of $\eta = 0.285$. This is a result, of course, of the fact that the parallel and transverse piezoelectric constants are of opposite signs. At this ratio of thickness to diameter, the two terms in the bracket of Equation (27) cancel each other.

51

E. Equivalent Circuit Analysis

The equivalent circuit (28) formulation for electromechanical transducers can also be used for the analysis of the barium titanate cylinders. In the circuit shown in Figure 22-a, a force with exponential decay, corresponding to the integrated pressure of the shock wave applied to the exterior surface of the cylinder, is applied to the mechanical terminals of the equivalent network through the characteristic impedance of the medium, assumed here to be purely resistive. The circuit constants L_m, C_m, and R_m are respectively the mass, compliance, and loss of the mechanical system. In this case R_m represents losses due to the mounting as well as internal mechanical losses in the titanate. The ideal transformer shown represents the electromechanical coupling between the mechanical and electrical meshes. On the electrical side of the transformer, C_e is the static or clamped capacitance of the cylinder, R_e represents the dielectric loss and R_e' is the shunt leakage resistance. The voltage V is the output voltage developed across the load resistance R_L.

Neglecting losses, and considering only the "open circuit" relation, the circuit of Figure 22-a can be transferred into the simpler form of Figure 22-b. The circuit constants of the system can be shown to be

$$C_e = \frac{0.6128\epsilon}{\log(b/a)} \tag{30}$$

$$N_a = b\left[g_{33}\left(\frac{a-b}{a+b}\right) - g_{31}\right] \tag{31}$$

$$C_v = \frac{2\pi L b^2}{Y}\left|\sigma - \frac{b^2 + a^2}{b^2 - a^2}\right| \tag{32}$$

$$k^2 = \frac{N_a^2 C_e}{N_a^2 C_e + C_v} \tag{33}$$

where N_a is the turns ratio of the ideal trasformer, C_v is the mechanical compliance, σ is Poisson's ratio, and the other terms are as before. The value for the turns ratio of the ideal transformer is seen to be identical with the equation for sensitivity derived in the preceding section, so that the analysis is essentially equivalent to that derivation. Values of C_e, N_a, C_v, k as a function of $\eta = t/d$ for cylindrical tubes of barium titanate are shown in Figures 23 through Figure 26.

The fundamental resonant frequency of the radial mode of the cylindrical tube is noticeably perturbed by elastic coupling to the length expander mode. This coupling effect is particularly marked in the region of length to diameter ratio of approximately 1.5. Figure 27 shows the relation between both the radial and length resonance as a function of length to diameter ratio. Below the critical point, the radial resonance frequency constant is about 53 kilocycle-inches per second.

F. Calculation of Frequency Response

With use of an equivalent circuit similar to those shown in Figure 22 and of a simplified stress function, Ehrlich (29) has derived a relation giving the open circuit voltage sensitivity of a barium titanate cylinder as a function of frequency. He includes electrical and mechanical losses as well as the effect of radiation load and derives the equation:

$$S(f) = \frac{2\pi aLY_{em}}{Y(f)\left[R_m + R_L + j(2\pi fM - \frac{k}{2\pi f})\right]} \qquad (34)$$

where $S(f)$ = the open circuit voltage response,

a = the mean radius of the cylinder,

L = length of cylinder,

Y_{em} = mutual admittance between the electrical and mechanical branches of the equivalent circuit,

$Y(f)$ = total admittance of the cylinder,

R_m = mechanical resistance of cylinder,

R_L = mechanical load resistance,

f = the frequency,

M = equivalent mass of cylinder, and

k = equivalent stiffness of cylinder.

The total admittance is given by:

$$Y(f) = 2\pi fc \tan \sigma + \frac{Y_{em}^2(R_m + R_L)}{|Z_m + Z_L|} + j\left[2\pi fc - \frac{Y_{em}^2(2\pi fM - \frac{k}{2\pi f})}{|Z_m + Z_L|^2}\right] \qquad (35)$$

where C = capacitance of cylinder,

σ = dielectric loss angle of the titanate,

Z_m = mechanical impedance of cylinder, and

Z_L = mechanical load impedance.

53

The following relationships can be shown to hold approximately:

$$C = 2\pi\epsilon a \frac{L}{b} \tag{36}$$

$$Y_{em} = 2\pi L d_{eff} Y_t \tag{37}$$

$$|Z_m + Z_L|^2 = (R_m + R_L)^2 + (2\pi f M - \frac{k}{2\pi f})^2 \tag{38}$$

$$R_m + R_L = 1.2 \ RL = 1.2\rho c(2\pi aL) \tag{39}$$

$$M = 2\pi ab L \rho_t \tag{40}$$

$$k = 2\pi b L Y_t \tag{41}$$

In the foregoing, the symbols have the following definitions:

ρ = density of the loading medium,

c = Sound velocity in the loading medium,

ρ_t = density of barium titanate,

Y_t = Young's modulus for barium titanate,

d_{eff} = "effective" piezoelectric modulus,

ϵ = dielectric constant for barium titanate, and

b = wall thickness of the cylinder.

The effective piezoelectric modulus depends on the ratio η of the wall thickness to diameter. It can be considered as given by:

$$d_{eff} = \left[d_{33} \left(\frac{\eta}{1-\eta} \right) + d_{31} \right] \tag{42}$$

Although the foregoing method for calculating frequency response is somewhat complicated in application, it has the advantage of yielding fairly accurate results through frequencies that include the first radial resonance and does include both electrical and mechanical losses in the titanate. Moreover, in the process of calculation, values are obtained for the complex impedance of the vibrating element. The analysis was developed originally for application to sonar transducers where the acoustic load ρc is equal to the acoustic resistance (1.55×10^5) of water. In applications to air blast gages where the acoustic resistance of the medium is small, mounting losses can be expected to control, and the calculated values at resonance are not expected to be accurate.

IV. DESIGN AND FABRICATION OF PENCIL GAGES

The application of the design formulas of the preceding section can be illustrated with applications to a specific case. For the calculations, it will be assumed that a gage design is required that has a flat frequency response from 1 cps to 100 kcps and that a transit time of not more than 15 microseconds for peak pressures of 10 psi is required. From these requirements and the preceding design information, the dimensions of a suitable barium titanate cylinder can be determined. Acoustical and mechanical requirements are contradictory and usually some compromise is necessary.

A. Design Calculations

The dimensions of the cylinder can be determined by the following procedure. To begin with, the transit time will determine the length of the cylinder and is readily found from the Rankine-Hugoniot equation. The shock velocity is seen to be about 1390 feet/second for a peak pressure of 10 psi. Hence

$$1 = \tau \cdot t = 1390 \times 12 \times 15 \times 10^{-6} = 0.25 \text{ inch} \qquad (43)$$

In order to obtain a flat frequency response to at least 100 kcps, the radial resonance will have to be somewhat higher, depending on the mechanical Q. The frequency constant for the radial mode, Figure 27, is 53 kilocycle-inches per second for short cylinders; so, for a frequency of 120 kcps, the mean diameter of the cylinder is 0.44 inch. The wall thickness is somewhat more arbitrary but ordinarily the highest sensitivity and capacitance is desired, which means as thin a wall as possible. This is often limited by the static pressure requirement of calibration apparatus, practical aspects of construction, or problems encountered in the vitrification of the barium titanate during manufacture. The latter limitation sets the minimum wall thickness for a cylinder of this size at about 0.04 inch. Cylinders of this wall thickness will withstand static pressure in excess of 500 psi.

A cylinder whose outside diameter is 0.50 inch and whose wall thickness is 0.040 inch has a ratio of wall thickness to outside diameter of 0.08. Figure 21 shows that the sensitivity, for a piezoelectric element of barium titanate with 5% calcium titanate additive, is approximately 3600 micro-microcoulombs per psi per inch length per inch diameter. If the cylinder is 0.25 inch long, the charge sensitivity is 3600 x 1/4 x 1/2 = 450 micro-microcoulombs per psi. For a barium titanate piezoelectric element, the

piezoelectric coefficients are greater by a factor of about 1.35 (see Table I); so the sensitivity would be about 600 micromicrocoulombs per psi. The ratio of length to mean diameter is 0.25/0.460 = 0.54. From Figure 27, the frequency constant is found to be 53 kilocycle-inches per second for the radial mode and 170 kilocycle-inches per second for the length mode, for barium titanate elements. The radial resonant frequency is 53/0.46 = 115 kcps and the length resonant frequency is 170/0.46 = 370 kcps. The capacitance, from Figure 23 is approximately 0.013 microfarads for a cylinder one inch long, or approximately 0.003 microfarads for a cylinder 1/4 inch long.

The low-frequency cut-off is determined by the RC time constant of the amplifier input circuit, where R is the combined leakage and load resistance and C is the total capacitance, including that of the gage, connecting cable, and the amplifier input. For the cylinder considered above, the response will be down 3 db at 1 cps if the load resistance is 53 megohms, assuming that the capacitance of the connecting cable is negligible and the leakage resistance is very great.

The gage parameters are all more or less interrelated. For example, the frequency response of the unit for the same transit time can only be increased at the expense of sensitivity, since the diameter would have to be decreased. Similarly a shorter transit time means a shorter cylinder and hence some loss in capacitance and charge sensitivity.

B. Mechnical Design and Fabrication

In the basic design, the cylinder is mounted on an insulated spindle and isolated from it by means of a corprene spacer. Neoprene and corprene washers further isolate the cylinder ends from the gage housing and the whole assembly is covered with a 1/16-inch neoprene sheath that is bonded to the active face of the cylinder and to the stainless steel housing as shown in Figure 28. A removable ogive nose is incorporated in one end of the gage while the other end terminates in a standard coaxial connector. A removable retaining ring serves as a mounting shoulder for use in the field as well as in the calibration chamber. The finished gage has a diameter of 5/8-inch and a length of 10 inches with the acoustic center of the sensitive element 3-1/2 inches forward of the retaining ring.

A neoprene cover protects the cylinder, eliminates water leakage, and markedly reduces pyroelectric effects (30) due to compressive heating of the shock.

In Figure 29-a the various parts of the gage are arranged in an exploded view. Figure 29-b shows the gage assembled and ready to be coated with neoprene.

A novel method has been developed for pressure molding the neoprene sheath at temperatures below the Curie point so that prepolarized cylinders can be employed. A solvent evaporation technique is used based on multiple coats of a neoprene cement with a 24-hour drying time between coats. The neoprene cement is approximately 20 percent solids, and a butyraldehyde aniline accelerator is used. The gage is mounted in a turning rack as shown in Figure 30 and four successive coatings of cement poured onto the turning gage. At approximately 50 rpm the optimum amount of cement is retained on the gage surface and evenly distributed during the solvent evaporation period. After·the final solvent evaporation period, the gage is inserted in a mold (see Figure 31) and cured for 24 hours at approximately 75°C. The result is a stock showing good aging, abrasion resistance, and tear resistance properties. It has a tensile strength of approximately 3000 psi, durometer hardness of 45, a density of 1.15 gms per cc, and a sound velocity of approximately 1500 m per sec. The elongation at rupture is in the vicinity of 450%.

The finished unit is shown in Figure 32-a. The model shown in Figure 32-b is electroacoustically similar to that shown in Figure 32-a, but the housing is somewhat longer and of a modified shape. It is intended for mounting in an extension tube.

C. Design Variations

There are a number of variations of the basic design. Figure 33-a shows a unit constructed with three barium titanate cylinders, spaced 4-1/2 inches apart. The center cylinder is mounted for measurement of transient pressures and the leads from this cylinder are brought out separately. The other two cylinders, intended for velocity measurement, have one common lead grounded to the housing; the other two leads are
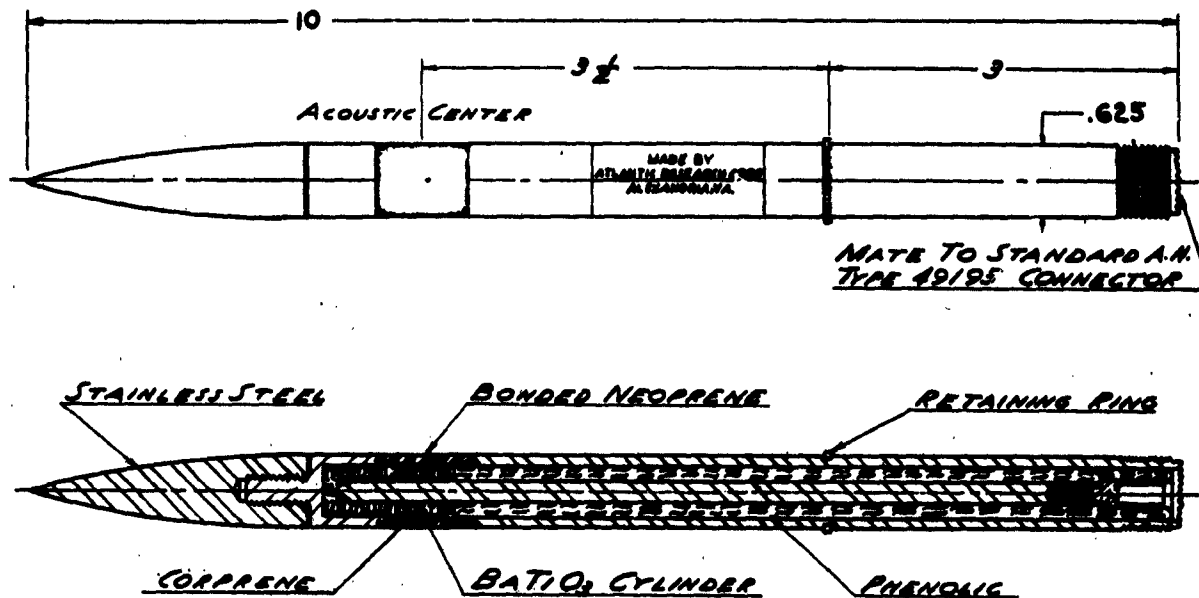
FIGURE 28: MECHANICAL DESIGN OF THE BARIUM
TITANATE PENCIL GAGE.

(A)

(B)

FIGURE 29: ASSEMBLY OF THE BARIUM
TITANATE PENCIL GAGE.

FIGURE 30: TURNING RACK FOR COATING THE
BARIUM TITANATE PENCIL GAGE.
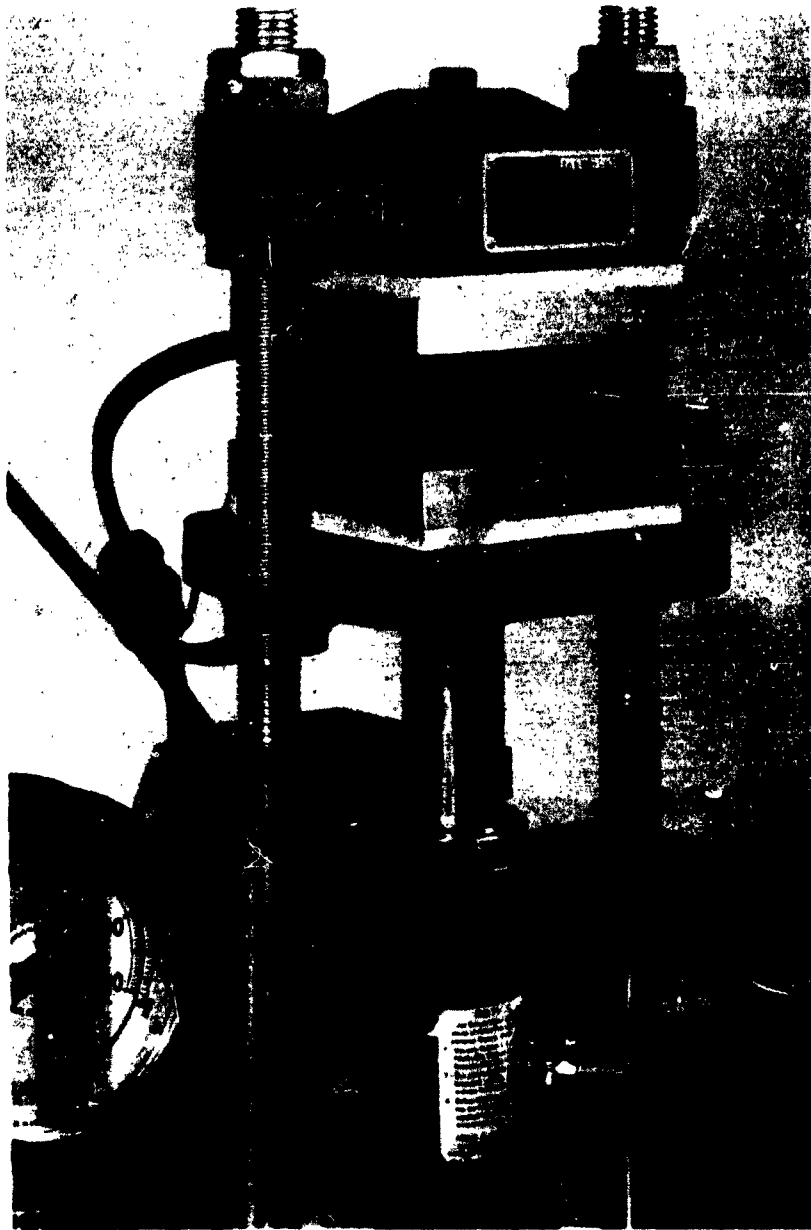
FIGURE 31 : MOLD AND PRESS FOR CURING THE
BARIUM TITANATE PENCIL GAGE.

(A)
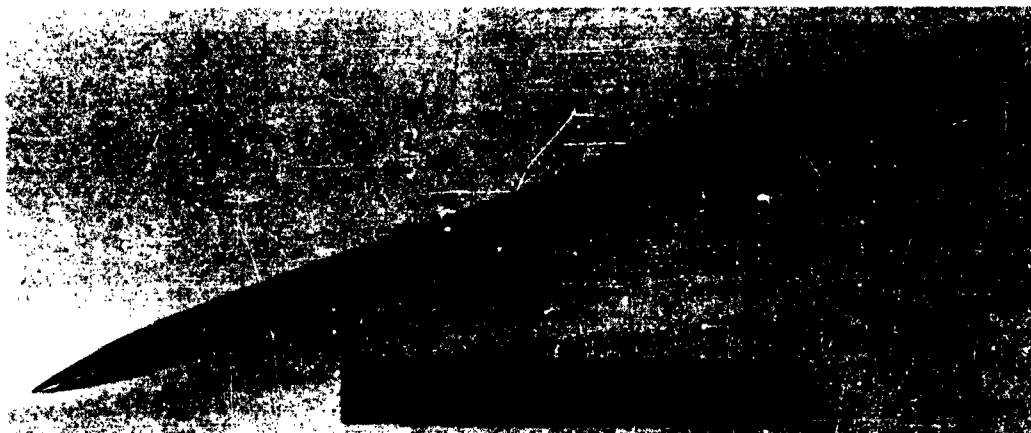
(B)

FIGURE 32 : CLOSE-UP VIEW OF COMPLETED
BARIUM TITANATE PENCIL GAGES.
(BRL PHOTOGRAPH)

brought out separately. The unit shown in Figure 33-b is a smaller version
using cylinders with 1/4-inch O.D., 1/32-inch wall thickness, andeither a
1/4-inch or 1/8-inch length. Units of this type have been used for free-field
blast pressure measurements, and, by mounting them in the wall surface, could
also be used to measure face-on pressures. There are, of course, a number of
other variations that can be designed using the procedures discussed above.

V. SUMMARY CHARACTERISTICS

In summary the average characteristics of pressure gages of this design
are as follows:

A. Physical Characteristics

In general, this transducer results in a rugged waterproof gage that is
capable of withstanding static pressures in excess of 500 psi and transient
pressures in excess of 1000 psi. The leakage resistances are well above 500
megohms even after immersion in water. Because of the mechanical isolation
of the barium titanate cylinder, the response of the blast pressure gage to
acceleration is less than 1 mv per g. Since the open circuit voltage
sensitivity to pressure is in the vicinity of 200 mv per psi response of
the unit to shock excited vibration is negligible in most instances.

B. Steady-State Response

Techniques for steady-state calibrations of transducers in air have not
yet been extended to frequencies as high as 100 kcps. However, so long as the
transducer is stiffness controlled, calibrations in a liquid will correspond
to the values obtained in air, except for the problem of diffraction. Gages
of the construction shown previously, using the 1/2-inch cylinder have been
calibrated in water using the techniques developed for sonar transducers.
Results are shown in Figure 34, together with calculated frequency responses
in both air and water using Equation (34). Agreement between measured values
and calculated values are good throughout most of the spectrum, although
there is some difference at the high-frequency end. This is a result of
loading by the neoprene coating, which introduces some losses and mass
loads the cylinder as well. The radial resonance of the gage is in the
vicinity of 95 kcps due to this mass loading (as compared to 120 kcps of
the unloaded cylinder). This effect can be eliminated by using a cylinder
having a thicker wall, but at the expense of sensitivity and capacitance.
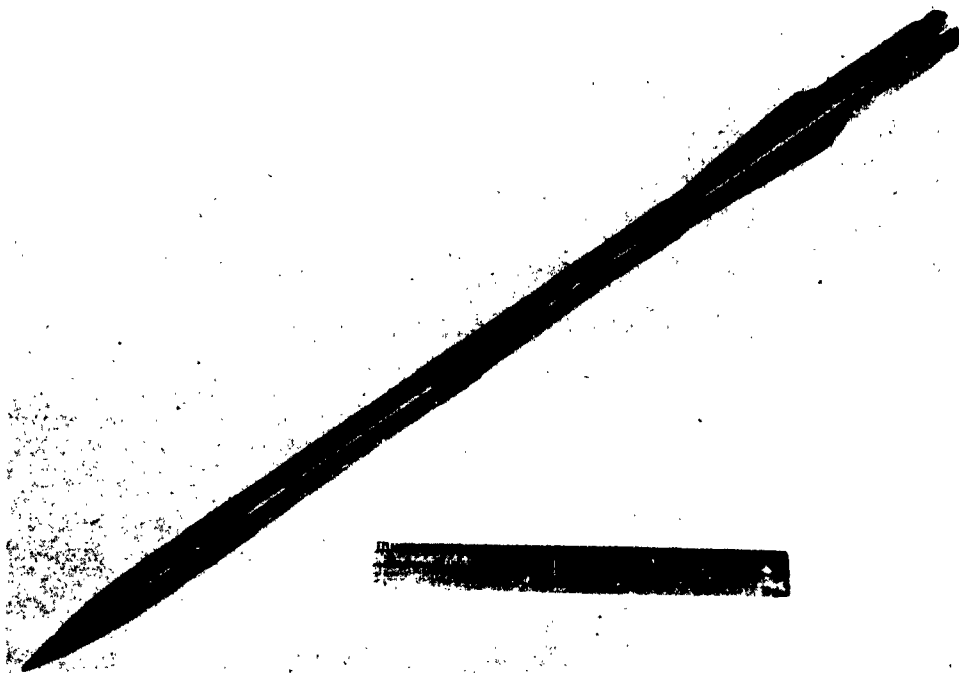
(A)
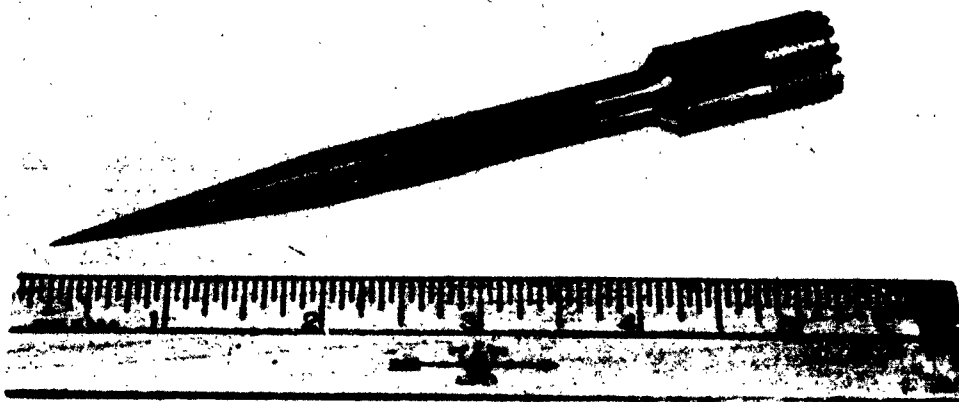
(B)

FIGURE 33: DESIGN VARIATIONS OF THE
BARIUM TITANATE PENCIL GAGE.
(BRL PHOTOGRAPH)
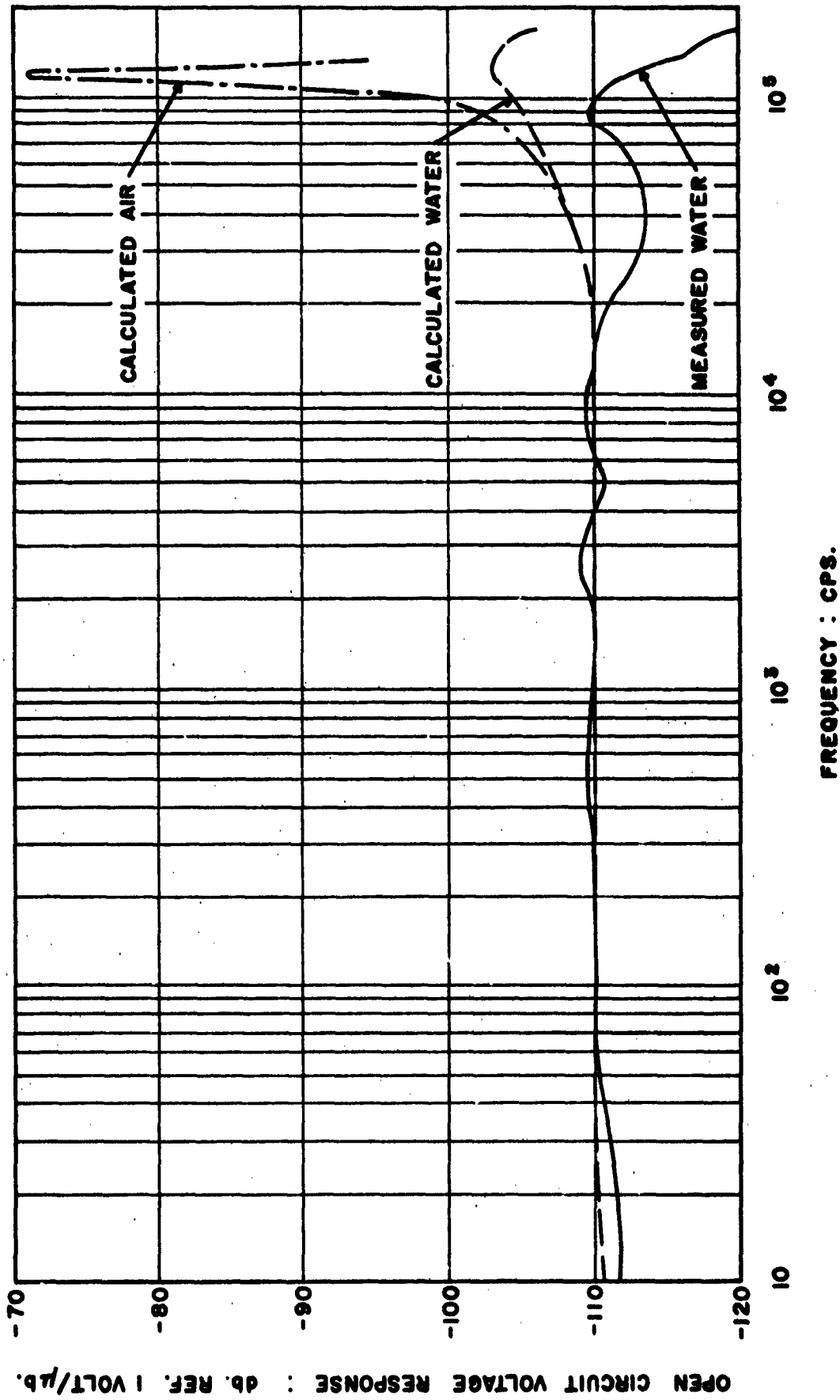
FIGURE 34 : CALCULATED & MEASURED FREQUENCY RESPONSE OF A BARIUM TITANATE PENCIL GAGE.

Figure 35 is a plot of the equivalent series resistance and reactance as a function of frequency. The characteristic excursion in the vicinity of 95 kcps is indicative of mechanical resonance. Figure 36 is a resonance-antiresonance curve of a cylinder before and after mounting. On the basis of these steady-state results some "ringing" at the resonant frequency can be expected in the response of the gage to a transient.

C. Transient Response

A typical pressure gage response is shwon in Figure 37. It was taken from an 8-pound charge of Pentolite. It shows the characteristic abrupt rise to peak pressure (in this case about 5 psi) followed by an exponential tail-off. Gages of this type not only reproduce peak pressures but also give a value for the initial slope for the decay curve that is within a few per cent of theoretical. The small variations near the peak of the trace correspond to the resonant ringing mentioned above.

D. Temperature Effects

Titanates used in most of the air blast gages fabricated during these studies used 5% calcium titanate additive. The dependence of sensitivity on temperature has been calculated from values of the piezoelectric constants measured at different temperatures. The calculated variation of sensitivity with temperature is compared with field data (31) in Figure 38. In using gages of this type over a wide temperature range, the curves of Figure 38 can be used to correct for the temperature effect.

Piezoelectric ceramic materials exist with less temperature dependence. These are being investigated by the Ballistic Research Laboratories. and will be the subject of a separate report.

VI. CONCLUSIONS AND RECOMMENDATIONS

In conclusion, it has been demonstrated that proper consideration of both aerodynamic and electroacoustic factors in air blast pressure measurements is important in gage design and development. Barium titanate cylinders properly mounted in pencil-shaped streamlined housings result in air blast gages capable of accurate reproduction of free-field shock-wave pressures. There are, however, a number of investigations remaining to be done that will lead to better understanding of the measurement problem and
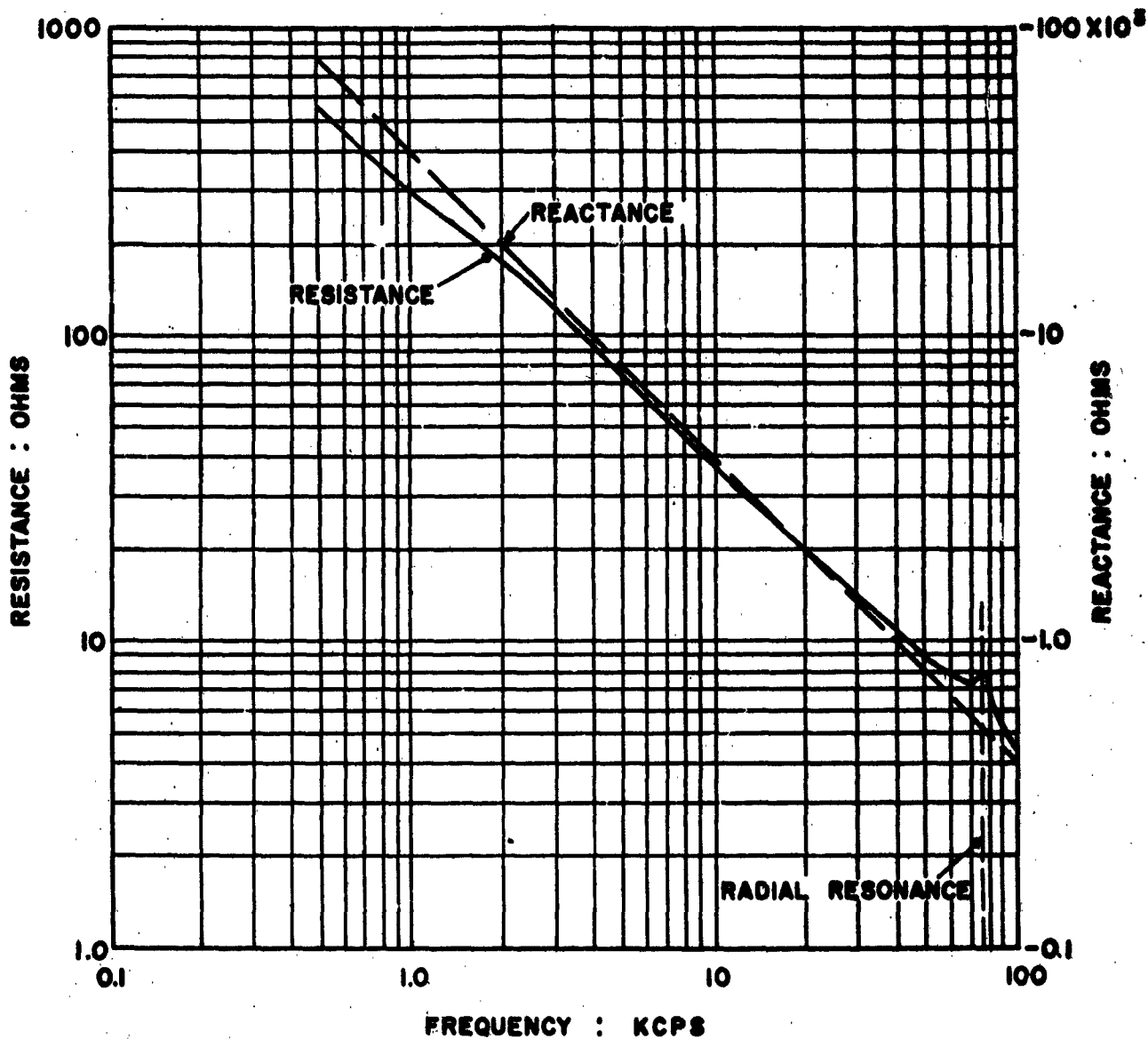
FIGURE 35 : VARIATION OF EQUIVALENT SERIES
RESISTANCE & REACTANCE WITH
FREQUENCY FOR THE BARIUM TITANATE
PENCIL GAGE.
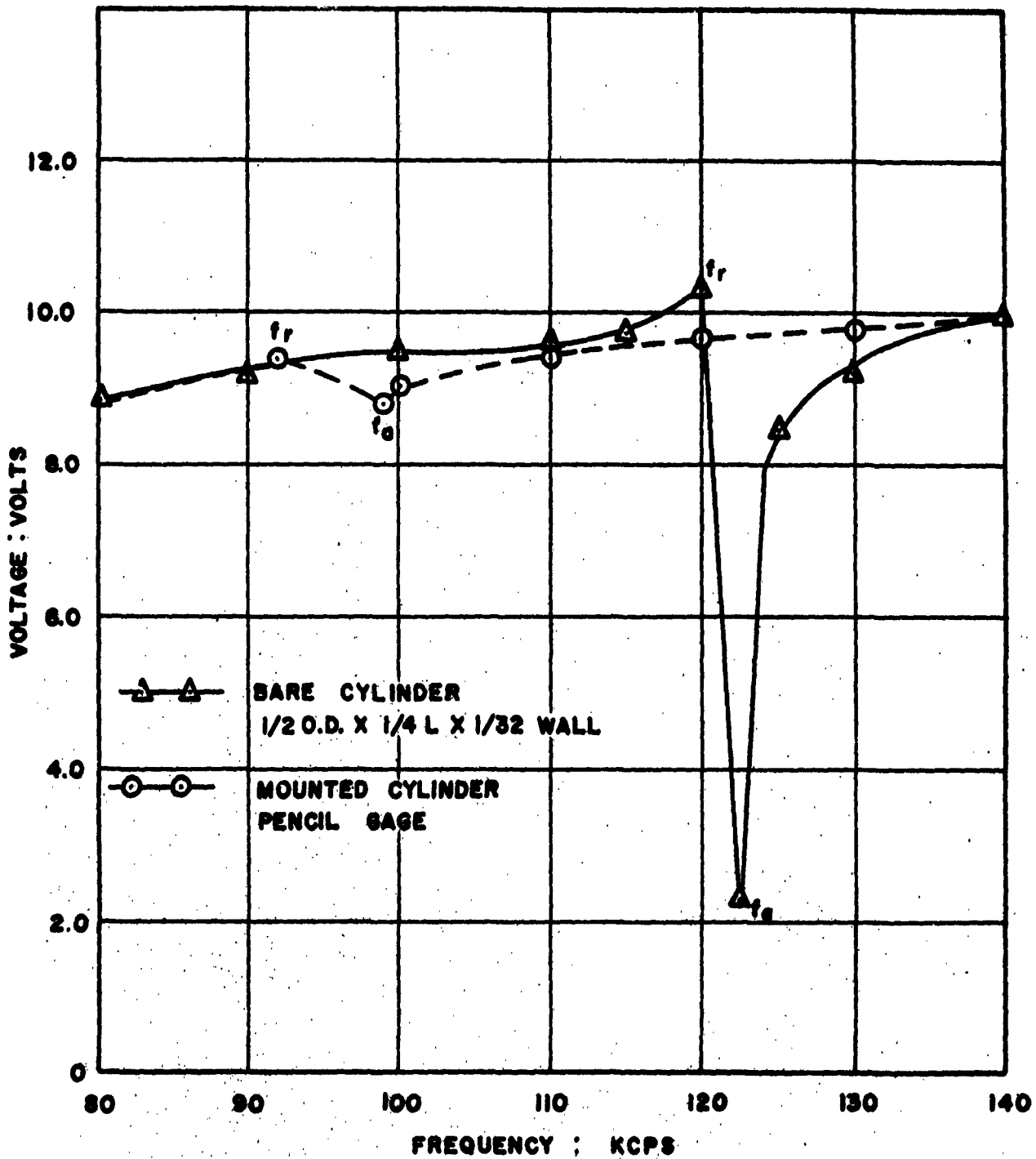
FIGURE 36: EFFECT OF CYLINDER MOUNTING ON RESONANT-
ANTIRESONANT CURVES.
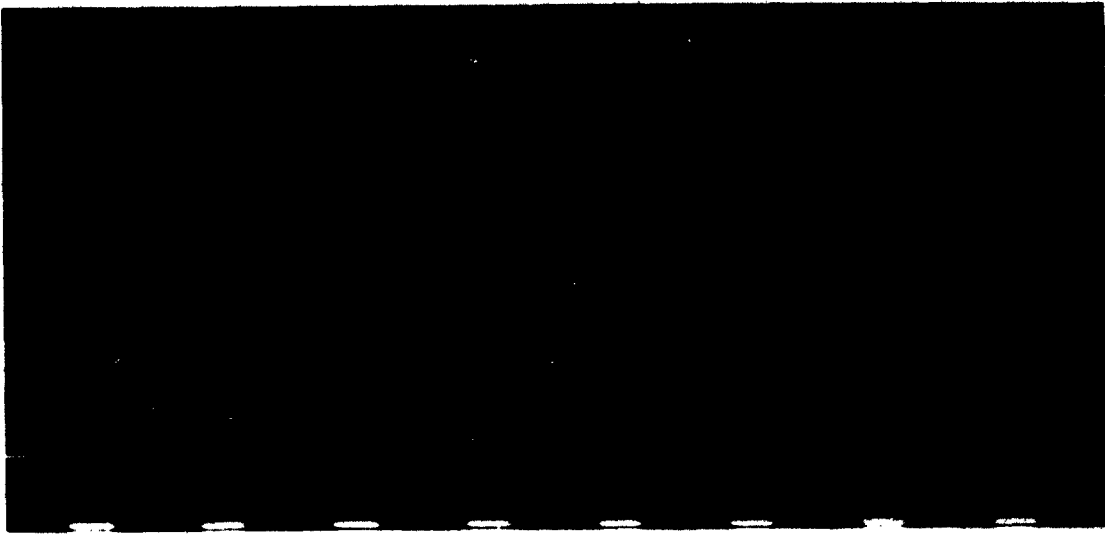
0° CHARGE - 5 PSI

FIGURE 37: TRANSIENT RESPONSE OF A BARIUM
TITANATE PENCIL GAGE.
(BRL PHOTOGRAPH)
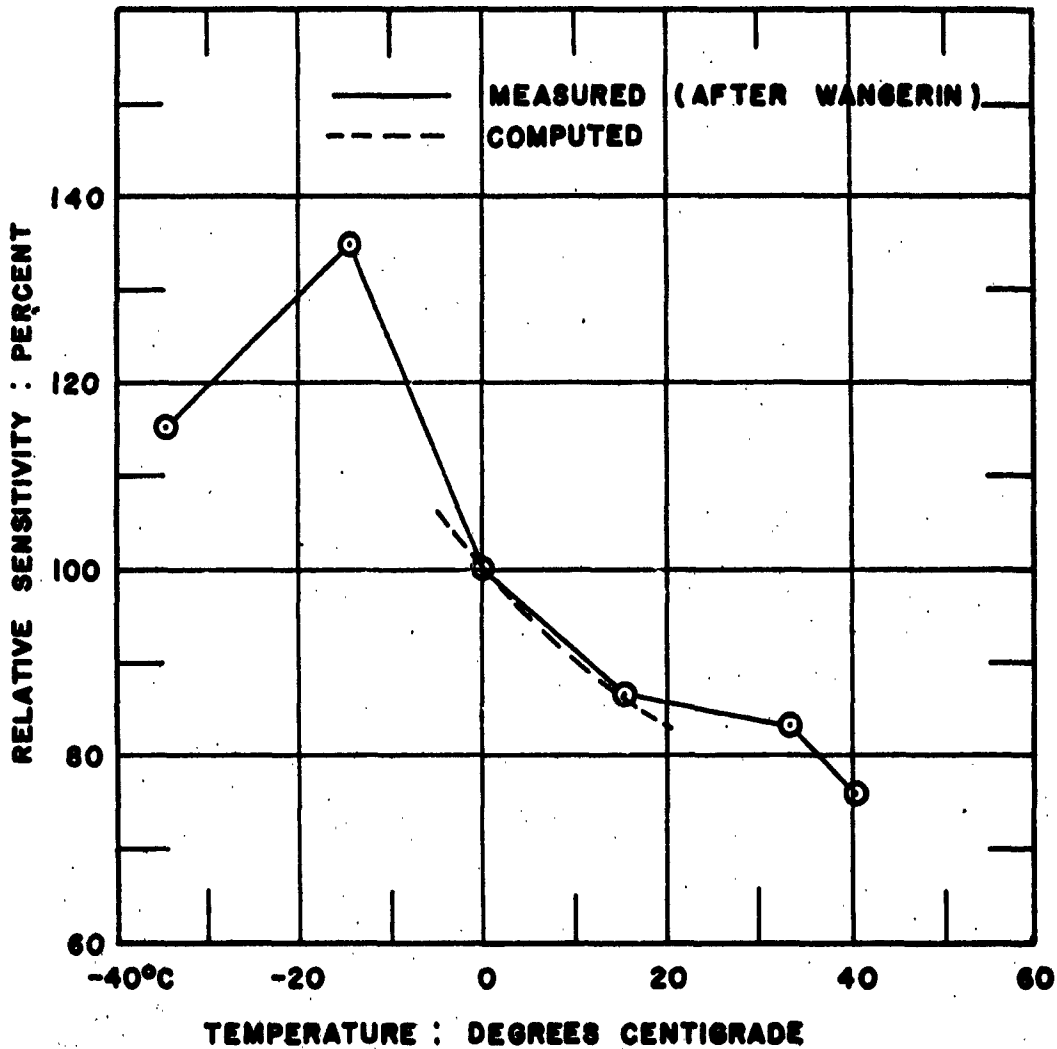
FIGURE 38 : VARIATION OF RELATIVE CHARGE
SENSITIVITY WITH TEMPERATURE;
BARIUM TITANATE PENCIL GAGE
WITH 5% CALCIUM TITANATE
ADDITIVE.

70

to gages of still better characteristics.

From the aerodynamic standpoint, further work needs to be done with gages in shock tubes at higher peak pressures and at various angles of incidence. In particular, the apparent negligible change in velocity of a shock traveling across pillbox housings seems inconsistent with response errors observed in the field. Concurrent field investigations of the angle of incidence should prove helpful.

If correlated with the aerodynamic studies, a more careful delineation of the electroacoustical characteristics of the gages being used would probably eliminate much of the unexplained phenomena of past measurements. Application of some of the newer titanate mixtures could substantially reduce temperature coefficients of sensitivity. For the practical aerodynamicist a series of charts and nomographs correlating aerodynamic and electroacoustic properties would be helpful.

One important area in the realm of air blast measurements not treated in this report is the problem of calibration. At the present time no method exists suitable for the absolute calibration of air blast gages. The three or four methods presently used are not consistent and rest on questionable foundations. There is a need for the establishment of reciprocity techniques to cover frequency ranges up to 100 kcps. In this connection the establishment of an Air Blast Measurement Reference Laboratory would be a major contribution.

REFERENCES

1. Contract DA-36-034-ORD-708RD.

2. Contract DA-36-034-ORD-708RD (Extension).

3. Contract DA-36-034-ORD-1126RD.

4. Atlantic Research Corporation; Design, Development, and Manufacture of Improved Transient Pressure Transducers; December 31, 1954. Technical Review Report prepared for Ballistic Research Laboratories.

5. J. W. Fitzgerald; The Characteristics of the Sk-H2 Hydrophones; September 1950, Confidential. U. S. Navy Underwater Sound Lab. Technical Memorandum 240.

6. R. H. Cole; Underwater Explosions; Princeton Univ. Press, 1945. p. 5.

7. R. Courant and K. O. Friedricks; Supersonic Flow and Shock Waves; Interscience, 1945.

8. A. H. Shapiro; Compressible Fluid Flow, Vols. I and II; Ronald Press, 1953.

9. C. W. Lampson; Resumé of the Theory of Plane Shock and Adiabatic Waves; BRL Technical Note 139, March 1950.

10. R. Courant and K. O. Friedricks; Ibid (7), p. 152-154.

11. R. Courant and K. O. Friedricks; Ibid (7). p. 327-328.

12. A. B. Arons and R. H. Cole; Design and Use of Piezoelectric Gauges for Measurement of Large Transient Pressures; Rev. Sci. Instr., Vol. 21, Jan. 1950.

13. T. D. Carr and M. A. Bakinowski; An Improved Tourmaline Air Blast Gage; BRL Report 397, 17 Oct. 1945.

14. J. K. L. MacDonald and S. A. Schaaf; On the Estimation of Per+ : ⋅tion Due to Flow around Blast Gages; AMG-NYU No. 136, NDRC, September 1945.

15. S. A. Schaaf; Estimation of Perturbations Due to Flow Around Blast Gages with Spheroidal Shapes; AMG-NYU No. 144, March 1946.

16. J. W. Hanna; A Pencil-Shaped Piezoelectric Air Blast Gage; BRL Technical Note 275, August 1950.

17. S. T. Marks; Response of Air Blast Gages of Various Shapes to One-Pound Spherical Pentolite Charges as a Function of Pressure Level; BRL Report 775, September 1951.

18. J. L. Barnes and M. F. Gardner; Transients in Linear Systems; Wiley, 1942.

19. R. H. Cole; Ibid (6), p. 200-203.

20. H. I. Oshry and J. M. Minkowski; Physical Properties of Piezoelectric Barium Titanate; Erie Resistor Corp. R. P. 30004.

21. NDRC; Summary Technical Report Div. 6, Vol. 13; The Design and Construction of Magnetostrictive Transducers; 1946.

22. The Brush Development Company; Technical Bulletin E-104, An Elementary Theory of Cylindrical Ceramic Transducers; January 1950.

23. W. P. Mason; Piezoelectric Crystals and Their Application to Ultrasonics; Van Nostrand, 1950.

24. H. Jaffe; Flectromechanical Properties of Titanate Ceramics; Brush Electronics Company, Brush Strokes, December 1951.

25. D. A. Berlincourt and F. Kulcsar; Electromechanical Properties of $BaTiO_3$ Compositions Showing Substantial Shifts in Phase Transition Points; Jour. Acoustical Society of America, Vol. 24, No. 6, November 1952.

26. W. P. Mason and R. F. Wick; Ferroelectrics and the Dielectric Amplifier; Proc. I.R.E., 42, 1606-1620 (1954).

27. R. A. Langevin; Electro-Acoustic Sensitivity of Cylindrical Ceramic Tubes; Jour. Acoustical Society of America, Vol. 26, No. 3, May 1954.

28. W. P. Mason; Electromechanical Transducers and Wave Filters; Van Nostrand, 1942.

29. S. Ehrlich; U. S. N. U. S. L. Memo Ser. 925-624, January 1951.

30. W. G. Cady; Piezoelectricity; McGraw-Hill, 1946.

31. C. J. Wangerin; The Effect of Ambient Temperature on Response of Air Blast Gages; BRL Memorandum Report No. 1003.

DISTRIBUTION LIST

No. of Copies	Organization	No. of Copies	Organization
	Chief of Ordnance Department of the Army Washington 25, D.C. Attn: ORDTB - Bal Sec ORDTA ORDTX-AR	1	Commanding Officer U. S. Naval Air Development Center Johnsville, Pennsylvania Attn: Mr. John D. Wallace
2	British Joint Services Mission 1800 K Street, N. W. Washington 6, D.C. Attn: Mr. John Izzard Reports Officer	1	Commanding Officer and Director David W. Taylor Model Basin Washington 7, D. C.
2	Canadian Army Staff 2450 Massachusetts Avenue Washington 8, D. C.	1	Commander Wright Air Development Center Wright-Patterson Air Force Base, Ohio Attn: Armament Laboratory
2	Chief, Bureau of Ordnance Department of the Navy Washington 25, D. C.	1	Commander Air Research and Development Command Post Office Box 1395 Baltimore 3, Maryland
1	Commander Naval Proving Ground Dahlgren, Virginia	1	Commander Air Force Armament Center Eglin Air Force Base, Florida Attn: Mr. William Neale
1	Commander Naval Ordnance Laboratory White Oak Silver Spring 19, Maryland Attn: Mr. Edward W. Fisher	1	Director Air University Maxwell Air Force Base, Alabama Attn: Air University Library
1	Commander Naval Ordnance Test Station China Lake, California Attn: Technical Library	1	U. S. Atomic Energy Commission Sandia Corporation Post Office Box 5900 Albuquerque, New Mexico
1	Commanding Officer and Director Naval Research Laboratory Washington 25, D. C. Attn: Code 2021	5	Director Armed Services Technical Information Agency Documents Service Center Knott Building Dayton 2, Ohio Attn: DSC-SD
1	Commanding Officer U. S. Naval Underwater Sound Laboratory New London, Connecticut Attn: Mr. D. E. Parker	1	Director U. S. Bureau of Mines Washington 25, D. C.

No. of Copies	Organization	No. of Copies	Organization
1	Director U. S. Bureau of Mines 4800 Forbes Street Pittsburgh 13, Pennsylvania Attn: Explosive Division	1	Armour Research Foundation 35 West 33rd Street Chicago 16, Illinois
1	Director National Bureau of Standards Washington 25, D. C.	5	Chesapeake Instrument Corporation Shadyside, Maryland Attn: Mr. James W. Fitzgerald
1	Chief of Engineers Department of the Army Washington 25, D. C.	1	Electronic Research Laboratory Tufts College Medford 55, Massachusetts Attn: Professor C. R. Mingins
1	Commanding General Frankford Arsenal Philadelphia 37, Pennsylvania Attn: Mr. C. M. Dickey	1	Dr. A. W. Hull Research Laboratory General Electric Company Schenectady, New York
1	Commanding General Redstone Arsenal Huntsville, Alabama Attn: Technical Library	1	Professor Walker Bleakney Palmer Physical Laboratory Princeton University Princeton, New Jersey
1	Commanding Officer Watertown Arsenal Watertown, Massachusetts	1	Office, Asst. Secretary of Defense (R&D) Committee on Ordnance Washington 25, D. C.
2	Commanding General White Sands Proving Ground Las Cruces, New Mexico Attn: ORDBS-TS-TIB	5	Atlantic Research Corporation Alexandria, Virginia
1	Deputy Chief White Sands Annex - BRL White Sands Proving Ground Las Cruces, New Mexico		
1	Commanding General Picatinny Arsenal Dover, New Jersey Attn: Mr. K. D. George		
1	Applied Physics Laboratory Johns Hopkins University Silver Spring, Maryland		